

ABSTRACT

Early Paleocene Plant Community and Paleoclimate Reconstruction of the Nacimiento Formation from the San Juan Basin, New Mexico

Danielle J. Gygi, M.S.

Mentor: Daniel Peppe, Ph.D.

Following the major extinction event at the Cretaceous-Paleogene (K-Pg) boundary, the Earth experienced a trend of long-term warming, punctuated by several short-term 'hyperthermal' events with associated carbon isotopic excursions in the early Paleogene. The early Paleocene climate record and the plant community response to the K-Pg extinctions and during and after hyperthermal events has been well studied in the northern Great Plains of North America but relatively little is known about the floral and climatic record at lower latitudes. The lack of data from terrestrial southern North American basins and from the middle Paleocene across North America limits our understanding of how Paleocene plant communities evolved and responded to climate change in the past and make it impossible to fully characterize regional patterns. This in turn inhibits our ability to understand how modern plant communities will respond to the unprecedented climate change the Earth is currently experiencing. The San Juan Basin in northwestern New Mexico and southern Colorado represents an ideal stratigraphic record for expanding our knowledge on plant community recovery and response to climate

change, because unlike other basins in North America, the San Juan Basin preserves a remarkable, nearly continuous, record of both fossil floras and mammalian turnover that spans the early and middle Paleocene. Additionally, the early Paleocene floral record collected from the Nacimiento Formation in the San Juan Basin has been well characterized and documents a flora that is considerably more diverse than the contemporaneous floras in North America.

Early Paleocene Plant Community and Paleoclimate Reconstruction of the Nacimiento Formation
from the San Juan Basin, New Mexico

by

Danielle J. Gygi, B.S.

A Thesis

Approved by the Department of Geosciences

Joe Yelderman, Ph.D., Chairperson

Submitted to the Graduate Faculty of
Baylor University in Partial Fulfillment of the
Requirements for the Degree
of
Master of Science

Approved by the Thesis Committee

Daniel Peppe, Ph.D., Chairperson

Steve Dworkin, Ph.D.

Joseph White, Ph.D.

Accepted by the Graduate School

May 2022

J. Larry Lyon, Ph.D., Dean

Copyright © 2022 by Danielle J. Gyi

All rights reserved

TABLE OF CONTENTS

LIST OF FIGURES	vi
LIST OF TABLES	ix
ACKNOWLEDGMENTS	x
DEDICATION	xi
CHAPTER ONE	1
Introduction.....	1
Geologic Setting.....	5
CHAPTER TWO	7
Methods	7
Fossil Collection and Classification.....	7
Stratigraphy and Magnetostratigraphy.....	8
Floral Diversity	10
Paleoclimate.....	11
CHAPTER THREE	12
Results.....	12
Floral Community Composition	12
Floral Diversity	13
Paleoclimate.....	16
CHAPTER FOUR.....	20
Discussion.....	20
Floral Composition and Diversity.....	20
Paleoclimate.....	21
Comparison to the Ojo Alamo Formation Floras	21
Regional Patterns of Floral Composition, Diversity, and Paleoclimate	23
CHAPTER FIVE	26
Conclusions.....	26
APPENDIX.....	28
Supplemental Data and Morphotype Descriptions	28
BIBLIOGRAPHY.....	83

LIST OF FIGURES

Figure 1.1. Early Paleocene terrestrial basins of North America	2
Figure 1.2. San Juan Basin geologic map and stratigraphy	4
Figure 2.1. Magnetostratigraphy of the San Juan Basin	10
Figure 3.1. Rarefaction curves of the Nacimiento Formation	14
Figure 3.2 San Juan Basin flora similarity dendrograms	16
Figure 3.3. Correlation of paleoclimate estimates to modern ecosystems.....	19
Figure 4.1. Nacimiento Formation temperature estimates through time	23
Figure A.1. Images of morphotype SJ-5	33
Figure A.2. Images of morphotype SJ-9	34
Figure A.3. Images of morphotype SJ-11	36
Figure A.4. Images of morphotype SJ-16	38
Figure A.5. Images of morphotype SJ-27	40
Figure A.6. Images of morphotype SJ-28	41
Figure A.7. Images of morphotype SJ-35	43
Figure A.8. Images of morphotype SJ-36	44
Figure A.9. Images of morphotype SJ-38	46
Figure A.10. Images of morphotype SJ-40	47
Figure A.11. Images of morphotype SJ-80	49
Figure A.12. Images of morphotype SJ-81	51
Figure A.13. Images of morphotype SJ-105	53

Figure A.14. Images of morphotype SJ-106.....	55
Figure A.15. Images of morphotype SJ-107.....	57
Figure A.16. Images of morphotype SJ-127.....	58
Figure A.17. Images of morphotype SJ-137.....	59
Figure A.18. Images of morphotype SJ-157.....	60
Figure A.19. Images of morphotype SJ-500.....	62
Figure A.20. Images of morphotype SJ-501.....	63
Figure A.21. Images of morphotype SJ-502.....	65
Figure A.22. Images of morphotype SJ-503.....	66
Figure A.23. Images of morphotype SJ-505.....	67
Figure A.24. Images of morphotype SJ-506.....	68
Figure A.25. Images of morphotype SJ-507.....	70
Figure A.26. Images of morphotype SJ-508.....	72
Figure A.27. Images of morphotype SJ-509.....	73
Figure A.28. Images of morphotype SJ-86.....	74
Figure A.29. Images of morphotype SJ-57.....	75
Figure A.30. Images of morphotype SJ-64.....	76
Figure A.31. Images of morphotype SJ-115.....	77
Figure A.32. Images of morphotype SJ-116.....	78
Figure A.33. Images of morphotype SJ-148.....	79
Figure A.34. Images of morphotype SJ-158.....	80
Figure A.35. Images of morphotype SJ-95.....	81
Figure A.36. Images of morphotype SJ-70.....	82

Figure A.37. Images of morphotype SJ-101	82
Figure A.38. Images of morphotype SJ-192	83

LIST OF TABLES

Table 3.1. Distribution and abundance of census floras	12
Table 3.2. Floral diversity statistics	15
Table 3.3. Bray-Curtis similarity	16
Table 3.4. Mean Annual Temperature estimates	17
Table 3.5. Mean Annual Precipitation estimates	18
Table A.1. Raw census data.....	30
Table A.2. Raw DiLP data.....	31

ACKNOWLEDGMENTS

I would like to acknowledge the Baylor Geoscience Department, the Baylor Graduate School, the Evolving Earth Foundation, the Colorado Scientific Society, the Paleontological Society, and the Dallas Paleontological Society for funding this research and presentations at conferences across the country. Additionally, this project would not have been possible without the help, guidance, and encouragement from my advisor Dr. Daniel Peppe. I would also like to acknowledge my first lab mate Dr. Joseph Milligan who helped me so much my first year at Baylor, I could not have done it without you. To Megan Lever and Venanzio Munyaka, thank you so much for all your help and assistance in the field and lab. To all my friends I made at Baylor, thank you for keeping me sane and creating a fun, welcoming community, I will miss you all. To my committee members, Dr. Steve Dworkin and Dr. Joseph White, thank you for all of your support and feedback on this project.

DEDICATION

To my mom: who always encouraged me to follow my dreams, even when it took me far away from you. I love you so much.

CHAPTER ONE

Introduction

The Paleocene floral record has been studied and documented in North America for over 150 years, often in relation to the recovery response after the mass extinction at the Cretaceous- Paleogene (K-Pg) boundary and long-term climate change (e.g., Newberry, 1868; Lesquereux, 1878; Knowlton, 1930; Brown, 1962; Hickey, 1977; Nichols and Ott, 1978; Hickey, 1980; Johnson, 1989; Wing et al., 1995; Manchester, 1999; Johnson, 2003; Dunn, 2003; Peppe, 2010; Flynn, 2020). Following the major extinction event at the Cretaceous-Paleogene (K-Pg) boundary, the Earth experienced a trend of long-term warming, punctuated by several short-term ‘hyperthermal’ events with associated carbon isotopic excursions in the early Paleogene, such as the late Danian event (LDE; ~62 Ma) and the Paleocene-Eocene Thermal Maximum (PETM; ~56 Ma.). The early Paleocene climate record and the plant community response to the K-Pg extinctions and during and after the PETM has been well studied in the Northern Great Plains of North America (Fig. 1; e.g., Johnson, 2002; Dunn, 2003; Wilf et al., 2003; Wilf and Johnson, 2004; Wing et al, 2005; Peppe, 2010; Wing and Currano, 2013; Lyson et al., 2019). However, many of the Paleocene floral records come from studies of the Bighorn, Hanna, Denver, and Williston basins, among others. Using the floral records from these more northern basins, it was demonstrated that Paleocene floras are low in diversity and relatively homogenous (Hickey, 1980; Johnson 2002; Barclay et al., 2003; Dunn, 2003; Peppe, 2010).

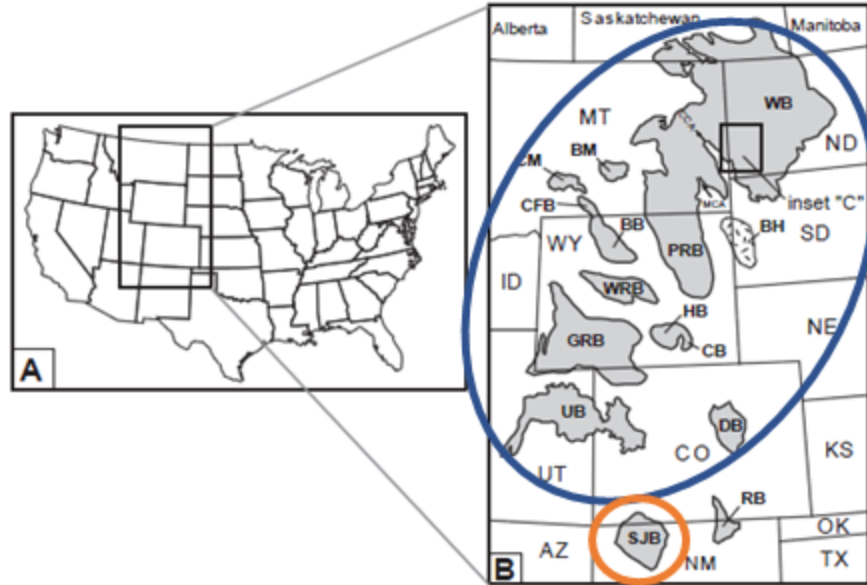


Figure 1.1. Map of early Paleogene terrestrial sedimentary basins in North America. Blue circle indicates the basins where the floral and climatic records have been relatively well characterized (particularly in the Williston Basin (WB), Bighorn Basin (BB), Hanna Basin (HB), and Denver Basin (DB)). The San Juan Basin (SJB), thus southernmost basin in the Western Interior of North America, is circled in orange.

Since this record was constructed primarily using basins in the Northern and Central Great Plains, it has left some gaps in the floral record in lower latitude basins, such as the San Juan Basin in New Mexico. This makes it difficult to access larger regional patterns of floral response and evolution to the K-Pg extinction, short-term hyperthermal events, and the patterns of climate change through the early Paleogene. Thus, it is critical to take into account these more southern terrestrial records in North America in order to fully understand the plant community response and recovery to the mass extinction and climate change, not only regionally, but latitudinally and temporally across North America. With the expansion of floral records in southern regions, it becomes possible to assess large scale patterns in floral diversity and their relationship to climate expands in the Paleocene. This in turn can help inform how modern plant

communities will respond and adapt to the unprecedented climate change the Earth is currently experiencing.

The San Juan Basin in northwestern New Mexico and southern Colorado represents an ideal stratigraphic record for expanding our knowledge of plant community recovery and response to climate change in the Paleocene, because unlike other basins in North America, the San Juan Basin preserves a remarkable, nearly continuous, record of both fossil floras and mammalian turnover that spans the early and middle Paleocene (Figure 2; e.g., Williamson, 1996; Flynn, 2020). Further, the chronostratigraphy for the Nacimiento Formation is well established (Leslie et al., 2018; Flynn et al., 2020), making it possible to determine the age of floral localities preserved through the Nacimiento Formation. Additionally, the early Paleocene floral record in the San Juan Basin from ~66 – 63 Ma has been well characterized (Flynn and Peppe, 2019; Flynn, 2020), and documents a flora that is considerably more diverse than the contemporaneous floras in North America. Further, climate reconstructions based on fossil leaves indicate that the early Paleocene San Juan Basin floras were characterized by a warm and wet climate that supported a tropical season forest to tropical forest biome (Flynn and Peppe, 2019), suggesting that the San Juan Basin samples a different climate regime than other more northern basins in North America. However, the floral record from the upper Nacimiento Formation is relatively unexplored, making it impossible to compare the middle Paleocene records across North America.

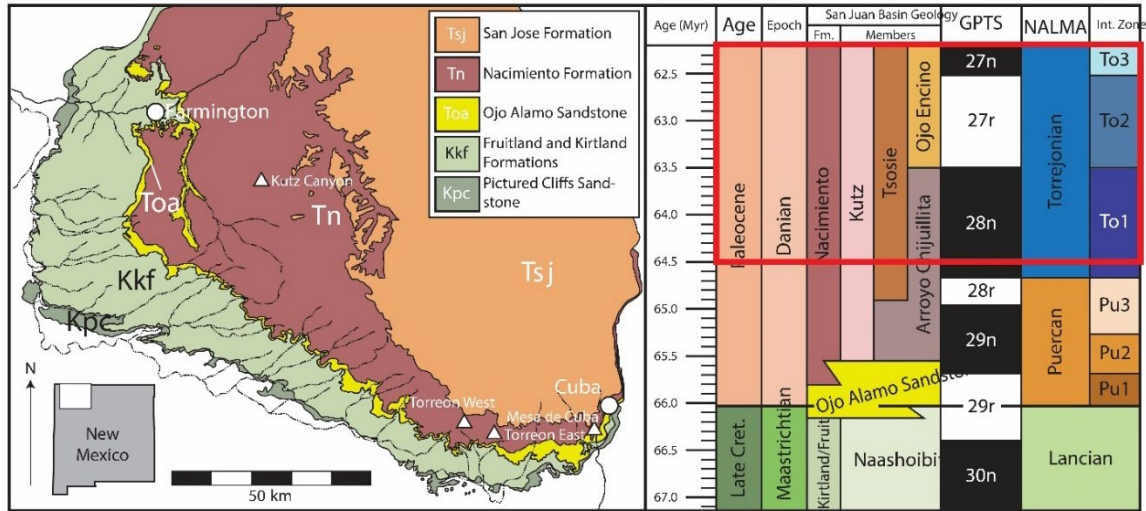


Figure 1.2. Geologic map of the San Juan Basin, New Mexico (modified from Williamson et al., 2008) showing the late Cretaceous through early Paleocene stratigraphy. Stratigraphy researched in this study is boxed in red. Fossil leaf localities and study sites are marked by white triangles.

To address this gap in the record, I will expand on the existing paleoclimate and plant community record within the San Juan Basin by collecting fossil leaves from the upper Nacimiento Formation in the San Juan Basin. This will make it possible to more completely reconstruct how lower latitude floras responded to the K-Pg boundary and long-term climate change. Further, I will compare the diversity and paleoclimate results from this study and to early and middle Paleocene floras the Bighorn, Hanna, Williston, and Denver Basins, which will provide insights into the latitudinal response of plant community response to extinction in the early Paleogene. These results will help provide crucial information needed for our understanding of how plant communities respond and adapt during and following mass extinctions and major climate change events.

Geologic Setting

The San Juan Basin is a Laramide foreland basin located in northwest New Mexico and southwest Colorado (see figure 1). The basin preserves a nearly continuous record of late Cretaceous to early Eocene deposits (Batzl et al. 1966; Chapin and Cather 1983) and is argued to have undergone three distinct phases of subsidence (Cather 2004). The initial phase occurred in the northeast region of the basin in the Campanian, ~78-75 Ma, followed by the second phase of northwest tilting and subsidence from the Campanian to the Maastrichtian, ~74-67 Ma. The third and final phase occurred in the northwestern part of the basin during the early Tertiary.

Within the basin, the Nacimiento Formation lies conformably over the Ojo Alamo Sandstone and unconformably underlies the Eocene San Jose Formation. Six members comprise the Nacimiento Formation: (1) The Kutz, (2) Tsosie, (3) Angel Peak, (4) Arroyo Chijuillita, (5) Ojo Encino, and (6) Escavada Members (Williamson and Lucas, 1992; Williamson, 1996; Cather et al., 2019). This study focuses on the Arroyo Chijuillita and Ojo Encino members from ages 64.5-62 Ma. The Arroyo Chijuillita Member ranges in thickness from 30-130 meters and consists of drab mudstone and interbedded lenticular fine sandstones with minor coal (Davis et al., 2016; Cather et al., 2019). The Ojo Encino Member is 90-122 meters thick and is identified by the repetition of black mudstones/paleosols, variegated red and green paleosols, and white cross-bedded sandstones (Williamson and Lucas, 1992; Williamson, 1996; Cather et al. 2019). The black mudstones are of specific importance because there are three distinct marker beds that can be traced around the basin, often referred to as the “lower,” “middle,” and “upper black” (Leslie et al., 2018b). Both members are confined to the southern portion

of the basin and are interpreted to be meandering fluvial systems with floodplain and channel deposits, with increasing depositional energy from the Arroyo Chijuillita to the Ojo Encino (Tidwell et al., 1981; Williamson, 1996; Davis et al., 2016; Cather et al., 2019; Flynn and Peppe, 2019). Regional dip of the Nacimiento Formation varies from 1-5°, but are locally flat lying (Batzl, 1967).

CHAPTER TWO

Methods

Fossil Collection and Classification

Plant fossils were collected from ten localities in the upper Nacimiento Formation of the San Juan Basin in New Mexico (Figure 1.1). Localities were named with the initials of the collector, a two-digit collection year indicator, and a two-digit site number (e.g., DG2102 is the second site found by D.G. in 2021). Sites DG2101-DG2106 were collected from Mesa de Cuba, DG2107-DG2109 are from Torreon West, and site DG2110 is from Torreon East (Figure 1.2).

Voucher collections were made at all fossil sites. The voucher collections were focused on collecting the best-preserved specimens and any unknown morphotypes.

Census collections were made at sites that had the best levels of preservation and most abundant fossils. In total, four census collections occurred at sites DG2102, DG2104, DG2109, and DG2110. When making census collections, at least 300 identifiable plant specimens were quantitatively tallied and sorted into respective morphotypes based on the gross morphology of the fossils. At least one representative specimen of each morphotype was collected, along with additional specimens that displayed the variation within the morphotype. Additionally, well-preserved specimens were also collected. During the census, all collected specimens were labeled with a site and specimen identification number (e.g., DG2102-C-46 denotes specimen 46 of the census collection at site DG2102), and the field morphotype was labeled on the rock

adjacent to the specimen and in field notes. All fossil specimens were wrapped in toilet paper, taped, labeled, and transported to Baylor University for further lab analyses.

All dicotyledonous angiosperm (dicots) fossil leaves were described using the ‘Manual of Leaf Architecture’ (Ellis et al. 2009). Monocotyledonous angiosperms (monocots) and ferns were primarily described and sorted according to venation patterns. Seeds and seed pods were grouped according to size and shape. From these descriptions, fossil specimens were organized into field morphotypes during census and voucher collections (e.g. Ellis et al. 2009; Peppe et al. 2008). In the lab at Baylor University, field morphotypes were reassessed in more detail, described in detail, and then correlated across all sites to create basin-wide morphotypes. See Supplementary Materials for descriptions of all morphotypes identified in this study.

Stratigraphy and Magnetostratigraphy

Four paleomagnetic block samples were collected from a single stratigraphic horizon at each census site. The positions of the localities were measured into the stratigraphic section using the black marker beds of the Ojo Encino member because of their consistent, basin-wide occurrence, allowing for basin-wide correlation. Samples were collected from mudstones, siltstones, and fine-grained sandstones; anything coarser than fine-grained sandstone was avoided. While the blocks were *in situ*, a flat face was shaved with a hand rasp and a strike and dip were measured on the flat surface with a Brunton compass. In the laboratory, the samples were cut using a diamond-bit rock saw into approximately 2 cm³ cubes, with each sample producing one cube.

Specimens were measured at Baylor University using a 2G Enterprises (Mountain View, California) cryogenic DC-SQUID magnetometer located in a two-layer

magnetostatic shielded room with a background field typically less than 300 nT. Thermal demagnetization steps were performed in 25-50°C increments to a maximum unblocking temperature or until the magnetizations became erratic and uncertain, which was typically around 300-450°C. To minimize oxidation reactions, thermal demagnetization was executed in a nitrogen atmosphere using ASC (Carlsbad, California) controlled atmosphere thermal demagnetizer. Based on the demagnetization trajectory, local polarity was assigned and then correlated to the broader magnetostratigraphic framework for the Nacimiento Formation (Figure 2.1; Leslie et al., 2018; Flynn et al., 2020).

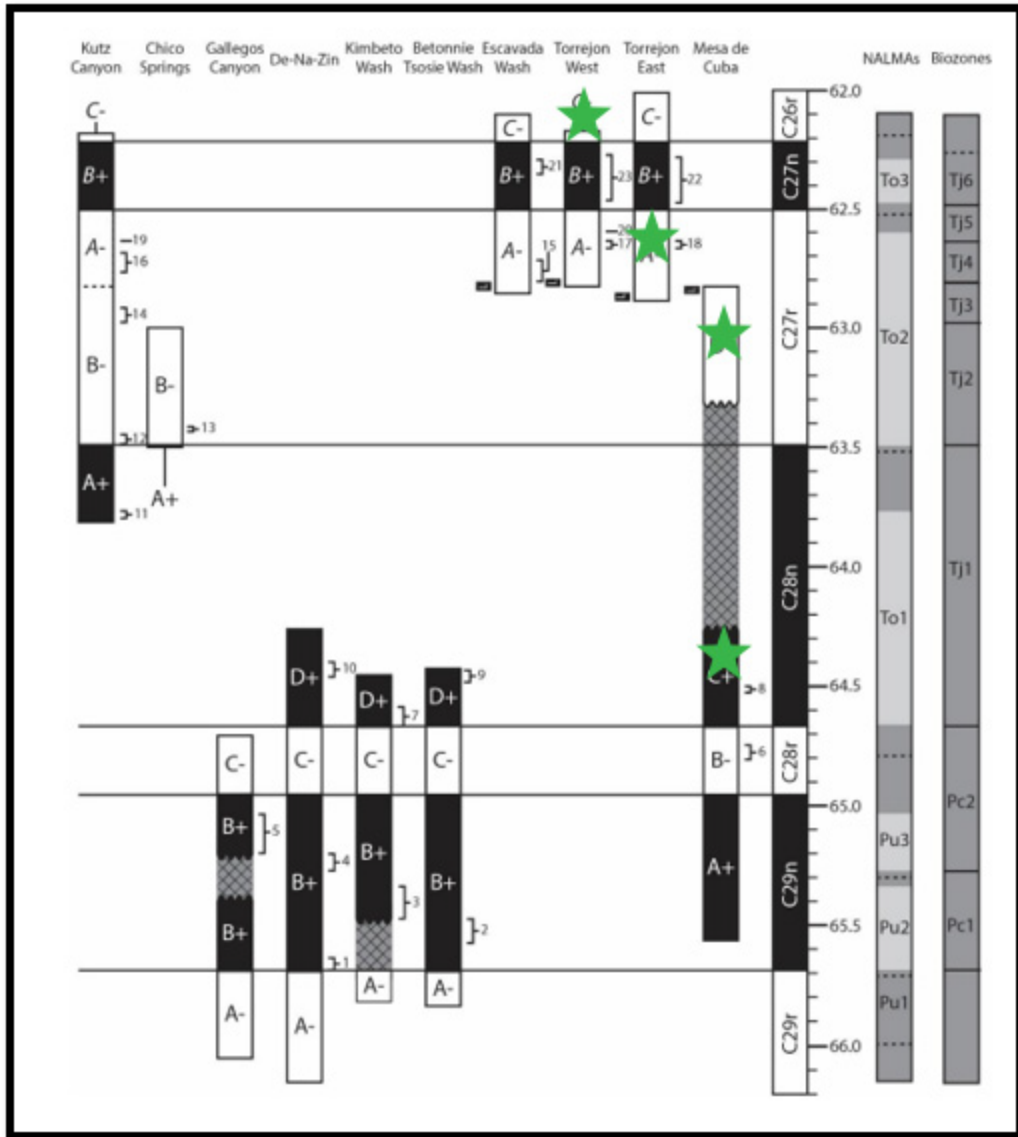


Figure 2.1. Magnetostratigraphy of the San Juan Basin. Green stars indicate where the fossil localities in this study are located within the polarity chrons.

Floral Diversity

Diversity and species richness analyses were performed for all morphotypes using the paleoecological statistical program PAST 3.0 (Hammer et al. 2001). Species richness was analyzed using quantitative census data from all census sites. Ecological diversity statistics were calculated for the same four census sites using abundance counts in order

to compare species richness, dominance, evenness, and similarity of the floras. Species richness, in addition to rarefaction curves, was estimated using the Chao-1 Index (Chao 1984). Evenness was assessed using Buzas and Gibson's evenness (1969). Dominance was calculated using the Simpson's Index and the Berger-Parker reciprocal (Simpson 1949; Berger & Parker 1970). Similarity was assessed using the Bray-Curtis measure (Legendre & Legendre 1998).

Paleoclimate

Univariant and multivariant paleoclimate proxies were used to estimate mean annual temperature (MAT) and mean annual precipitation (MAP) at all census sites. Leaf margin analysis (LMA) is a univariant climate proxy that uses the presence or absence of teeth in woody dicot angiosperm leaves to reconstruct MAT (Wilf 1997; Miller et al. 2006; Peppe et al. 2018). Leaf area analysis (LAA) is another univariant paleoclimate proxy that uses average leaf area of a floral to determine MAP (Wilf et al. 1998; Peppe et al. 2011). Digital leaf physiognomy (DiLP) is a fully digital, multivariate method that uses climatically driven leaf traits to estimate MAT and MAP (Huff et al. 2003; Royer et al. 2005; Peppe et al. 2011). For DiLP analyses, all fossil woody dicot leaves with $\geq 25\%$ preservation were measured using the protocols outlined in Royer et al. (2005) and Peppe et al. (2011).

CHAPTER THREE

Results

Floral Community Composition

Fossil floras collected from the Nacimiento Formation generated a total of 39 morphotypes, 27 of which were dicot leaves. Pteridophytes made up six morphotypes, two were monocots, one lycophyte, and three dicot reproductive structures. Of the total specimens counted, 15.02% were pteridophytes, 0.09% lycophytes, 3.59% monocots, 81.11% dicot leaves, and 0.19% dicot reproductive structures. See Table 3.1 for full breakdown of abundance and distribution data for the census sites.

Table 3.1. Abundance and Distribution of Census Morphotypes

Higher Taxon		Morphotypes	Specimens	% Morphotypes	% Specimens
<i>Pteridophytes</i>		6	318	15.38	15.02
<i>Lycophytes</i>		1	2	2.56	0.09
<i>Monocotyledonous Angiosperms</i>		2	76	5.13	3.59
<i>Dicotyledonous Angiosperms</i>	Leaves	27	1717	69.23	81.11
	Seeds	3	4	7.69	0.19
Total		39	2117		

Census collection DG2102 yielded a total of 15 morphotypes from 588 fossil specimens, consisting of 73% dicots, 14% ferns and fern allies, 7% monocots, and 7% seeds. Of the 73% dicots, 27% were toothed. SJ-105 (San Juan morphotype 105) made up 42% of the specimen count.

For collection DG2104, 607 specimens were tallied and nine morphotypes were recorded, of which 67% were dicots, 22% ferns and fern allies, and 11% seeds. 50% of

the dicot leaves were toothed. The collection was dominated by SJ-500 which accounted for 90% of the counted specimens.

Census DG2109 consisted of 401 specimens and 14 morphotypes. Of the morphotypes, dicots accounted for 79%, seeds were 14% and monocots totaled 7%. 27% of the dicots had toothed margins. Morphotype SJ-40 comprised 33% of the collection.

Census DG2110 generated 15 morphotypes from 521 specimens, consisting of 73% dicots, 20% ferns and allies, and 7% seeds, with 27% of dicots having teeth. The most abundant morphotype was SJ-158, which accounted for 40% of the collection.

Several of the morphotypes are present at multiple sites, but none appear at all four. 20.51% of the morphotypes appear at two sites while 7.69% occur at three sites. Morphotypes SJ-11, SJ-506, and SJ-28 are present at DG2102, DG2110, and DG2109 while SJ-507 was present at DG2102, DG2104, and DG2109. SJ-40 and SJ-80 are recorded at sites DG2110 and DG2109 and SJ-27 and SJ-192 are at both DG2102 and DG2104. Site DG2110 shares SJ-105 with DG2102 and SJ-64 with DG2104.

Floral Diversity

The total number of morphotypes at sites DG2102 and DG2110 is 15, DG2109 with 14, and DG2104 having only 9. Rarefaction curves for sites DG2102 and DG2110 indicate similar species richness of 14 morphotypes, but DG2110 does not fully plateau, indicating that total species richness at the site may not have been fully sampled (Figure 3.1). DG2109 has lower species richness with 12 morphotypes, but also does not reach an asymptote (Figure 3.1). Rarified richness at DG2104 was 8 morphotypes, and the rarefaction curve plateaued, suggesting the richness was well sampled (Figure 3.1). When down sampled to a sample size of 400, site DG2102 has a rarefied richness of $14.06 \pm$

0.84, DG2104 is 8.29 ± 0.69 , DG2110 is 14.07 ± 0.84 , and DG2109 is 13.99 ± 0.10 . The Chao-1 Index for all sites estimate a larger number of species at each site, another indication our sites were not fully sampled. The Chao-1 Index estimates for sites DG2102, DG2104, DG2110, and DG2109 are 15.25, 10.00, 21.00, and 15.50, respectively (Table 3.2)

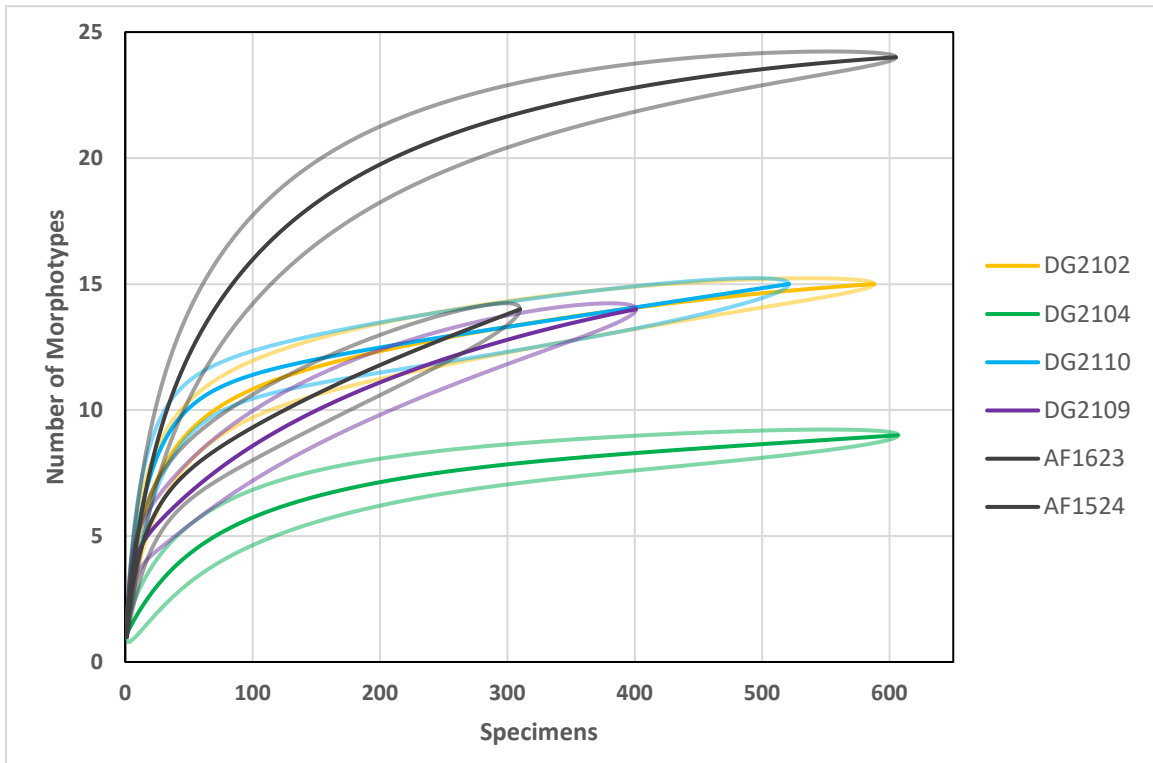


Figure 3.1. Rarefaction curves using all identified vegetative plant organs from six census localities in the SJB; envelopes indicate 95% confidence intervals. Grey curves indicate census localities from Flynn 2020 from the older Nacimiento Formation. Colored curves are localities from this study, all of which have lower or similar species richness to the older floras.

Table 3.2. The number of taxa, the total tally for each census collection, and a range of diversity statistics including dominance, evenness, Berger-Parker Reciprocal, and Chao-1 index. Included are all of the collections in this study and previous collections from older strata. (Buzas & Gibson 1969; Berger & Parker 1970; Chao 1984)

	DG2102	DG2104	DG2110	DG2109	AF1623	AFG1524
<i>Taxa</i>	15	9	15	14	24	14
<i>Individuals</i>	588	607	521	401	605	310
<i>Dominance</i>	0.241	0.809	0.211	0.231	0.279	0.364
<i>Evenness</i>	0.410	0.184	0.477	0.370	0.301	0.311
<i>Berger-Parker Reciprocal</i>	2.380	1.114	2.505	3.061	1.984	1.751
<i>Chao-1</i>	15.25	10.00	21.00	15.50	24.20	29.00

There are notable differences in the diversity of the different census sites. For example, site DG2104 is the least diverse of the sites and has the highest dominance of a single species (Table 3.2). Site DG2109 has the highest Berger-Parker reciprocal, indicating the highest level of diversity (Table 3.2) out of all the sites. Site DG2110 has the most even distribution of species (Table 3.2).

While all sites are markedly different in composition from one another, there are some overlaps in morphotype occurrences. Sites DG2109 and DG2110 have the highest Bray-Curtis similarity value of 0.235, followed by sites DG2102 and DG2110 with a value of 0.145 (Table 3.3, Figure 3.2). The similarity indices are more similar by facies, not time.

Table 3.3. Bray-Curtis Similarity.

<i>Site</i>	<i>DG2102</i>	<i>DG2104</i>	<i>DG2110</i>	<i>DG2109</i>	<i>AF1623</i>	<i>AF1524</i>
<i>DG2102</i>	1	0.005	0.142	0.095	0.049	0.016
<i>DG2104</i>	0.005	1	0.002	0.008	0.000	0.002
<i>DG2110</i>	0.142	0.002	1	0.234	0.053	0.132
<i>DG2109</i>	0.095	0.008	0.234	1	0	0.003
<i>AF1623</i>	0.049	0.000	0.053	0	1	0.238
<i>AF1524</i>	0.016	0.002	0.132	0.003	0.238	1

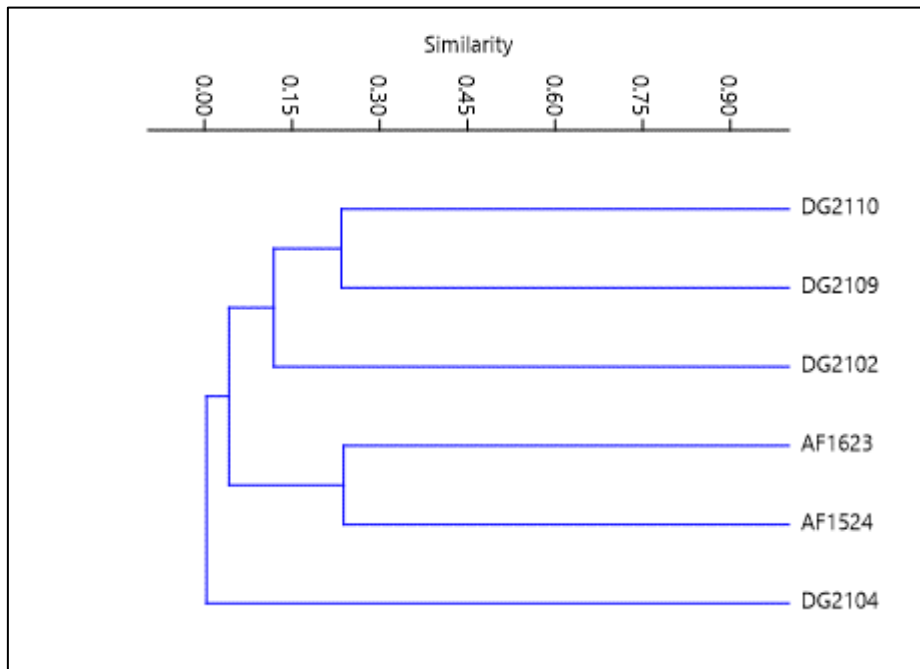


Figure 3.2. Dendrograms of the SJB census floras showing how similar or dissimilar the collections are.

Paleoclimate

MAT was reconstructed for sites DG2102, DG2109, and DG2110 using three LMA models. DG2104 was excluded from these analyses due to a small total number of morphotypes present at the site ($n = 9$). Due to the same proportion of toothed to entire margins being present at all other sites, DG2102, DG2109, and DG2110 all record the

same MAT: $16.8 \pm 4.1^\circ\text{C}$, $15.5 \pm 4.8^\circ\text{C}$, and $16.2 \pm 4.54^\circ\text{C}$ using the Miller et al. (2006), Peppe et al. (2011), and Peppe et al. (2018) models, respectively (Table 3.3). Due to a lack of enough well-preserved specimens to make a DiLP MAT estimate for each site, instead leaf physiognomic measurements were combined from all individual sites to create a grand mean MAT of $16.375 \pm 4^\circ\text{C}$, which is similar to the LMA estimates of MAT.

Table 3.4. Mean Annual Temperature Estimates.

Site	Leaf Margin Analysis						Digital Leaf Physiognomy	
	Miller et al. (2006)	Error	Peppe et al. (2011)	Error	Peppe et al. (2018)	Error	Grand Mean MAT	Error
<i>DG2102</i>	16.8	± 4.1	15.5	± 4.8	16.2	± 4.54		
<i>DG2110</i>	16.8	± 4.1	15.5	± 4.8	16.2	± 4.54	17.1	± 4
<i>DG2109</i>	16.8	± 4.1	15.5	± 4.8	16.2	± 4.54		

MAP was reconstructed for all sites using three LAA regression models (Wilf et al., 1997; Peppe et al., 2011; Peppe et al., 2018). Site DG2102 MAP estimates were 228.8 cm/yr ($+98.8/ -69.0$), 206.6 cm/yr ($+173.7/ -94.4$), and 210.5 cm/yr ($+137.9/ -83.3$) using Wilf et al. (1997), Peppe et al. (2011), and Peppe et al. (2018), respectively. DG2104 recorded MAPs of 191.2 cm/yr ($+82.6/ -57.7$), 188.6 cm/yr ($+158.5/ -86.1$), and 187.9 cm/ yr ($+123.1/ -74.4$). MAP for DG2110 was 155.9 cm/yr ($+67.3/ -47.0$), 170.0 cm/ yr ($+142.9/ -77.6$), and 165.2 cm/ yr ($+108.3/ -65.4$). MAP at DG2109 were estimated at 154.1 cm/ yr ($+66.6/ -46.5$), 169.0 cm/yr ($+142.0/ - 77.2$), and 164.0 cm/yr ($+107.5/ -$

64.9). The DiLP grand mean MAP for all sites was 152.175 cm/ yr (+125.125/ -68.675) (Figure 3.5).

Using the DiLP grand mean MAT and MAP estimates, the floras from the upper Nacimiento Formation indicate a temperate forest biome (Figure 3.3, Whittaker 1975).

Table 3.5. Mean Annual Precipitation Estimates.

Site	Leaf Area Analysis						Digital Leaf Physiognomy	
	Wilf et al. (1997)	Error	Peppe et al. (2011)	Error	Peppe et al. (2018)	Error	Grand Mean MAP	Error
<i>DG2102</i>	228.8	(+98.8 /-69.0)	206.6	(+173.7 /-94.4)	210.5	(+137.9 /-83.3)	146.5	(120.4/-66.1)
<i>DG2104</i>	191.2	(+82.6 /-57.7)	188.6	(+158.5 /-86.1)	187.9	(+123.1 /-74.4)		
<i>DG2110</i>	155.9	(+67.3 /-47.0)	170.0	(+142.9 /-77.6)	165.2	(+108.3 /-65.4)		
<i>DG2109</i>	154.1	(+66.6 /-46.5)	169.0	(+142.0 /+77.2)	164.0	(+107.5 /-64.9)		

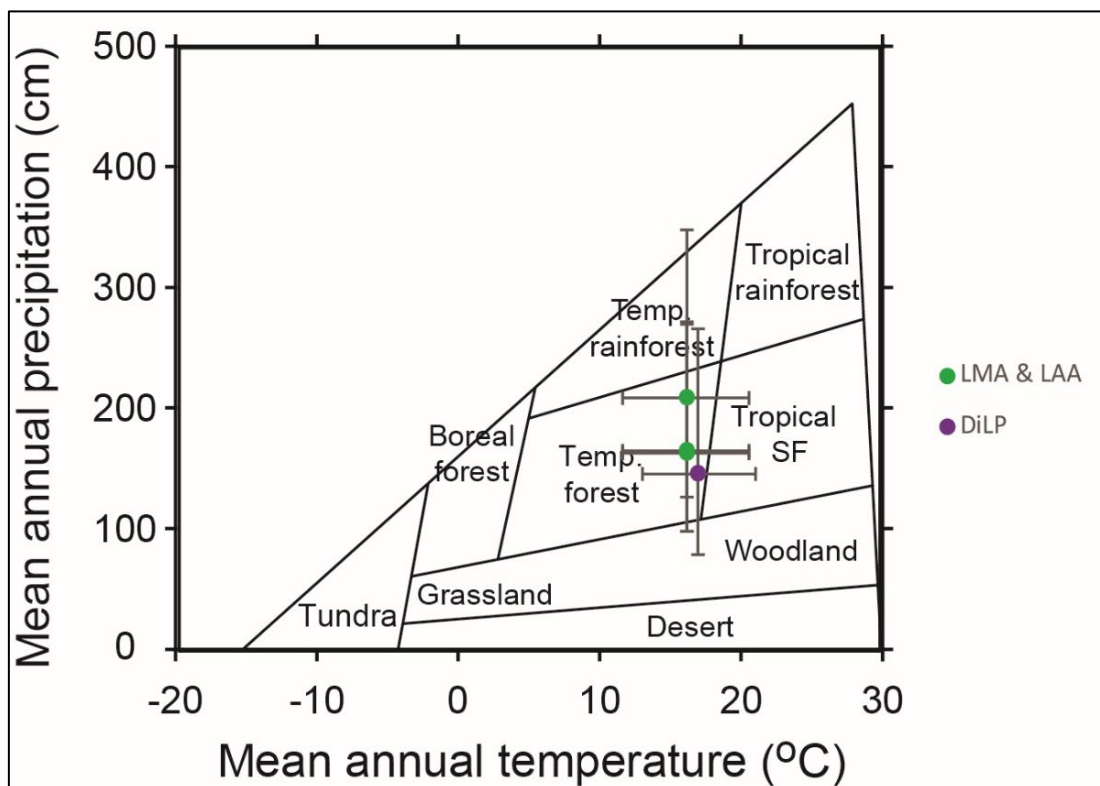


Figure 3.3. Modern ecosystem plot with paleoclimate variables. The SJB floras in this study plot within modern temperate forest to rainforest to seasonal tropical forest using both multivariate and univariate paleoclimate proxies (Whittaker 1975).

CHAPTER FOUR

Discussion

Floral Composition and Diversity

The plant communities of the San Juan Basin are dominated by dicot angiosperms, making up 81.11% of the specimens and 69.23% of the morphotypes found. Pteridophytes are quite common (15.02% of specimens and 15.38% of morphotypes). Monocots are also common, but to a lesser degree (3.59% of specimens and 5.13% of morphotypes). Lycophytes are rare in the floral record, only comprising 0.09% of specimens and 2.56% of morphotypes. No conifers were identified in this study.

Excluding site DG2104, all other sites have relatively similar number of morphotypes and are comparable in dominance and evenness. Additionally, DG2102, DG2109, and DG2110 all exhibit an equivalent species richness shown by their respective rarefaction curves (see Figure 3.1). DG2104 is well below the other sites in species richness due to only having eight morphotypes present. DG2102, DG2104 and DG2110 rarefaction curves signify that the sites have been well sampled, indicated by their asymptotic nature. DG2109 has not been as fully sampled, shown by its steeper rarefaction curves. Despite sites DG2102, DG2109, and DG2110 having diversity levels mirroring each other, the sites display very low Bray-Curtis similarity levels, indicating that all of the sites are markedly different in composition from each other (see Figure 3.2). As an example of the considerable difference between the sites, out of 39

morphotypes identified in this study, only eleven of them occur at more than one census locality.

Comparisons between the sites suggest that there is a considerable facies effect due to a taphonomic filter on the Nacimiento floral diversity and composition, which is best illustrated by site DG2104. It is the only channel facies that was censused and has the lowest species richness of all census sites and is extremely dominated by one morphotype. This is unlike the other three sites that were overbank deposits and are significantly more even in their morphotype distribution. Additionally, the dominant morphotype at DG1204 did not occur at any of the other sites.

Paleoclimate

Mean annual temperature (MAT) and mean annual precipitation (MAP) estimates for the SJB plant communities sampled in the study reconstruct the biome of the floras to have been a temperate forest to temperate rainforest to tropical seasonal forest, indicating mesic conditions, and likely seasonal variation in precipitation (Figure 3.3). Generally, the same climatic conditions were observed across all sites, and the MAT and MAP estimates from all of the sites overlap within uncertainty. The univariate MAT and MAP estimates are similar to the grand mean DiLP estimates of climate; however, some caution is needed when interpreting the DiLP results because the vast majority of specimens used in the analyses were fragmentary, which may unintentionally bias the DiLP climate estimates.

Comparison to the Ojo Alamo Formation Floras

In the Ojo Alamo Formation (~66.1-65.5 Ma) of the SJB, fossil collections totaled 55 morphotypes, with 2939 specimens for quantitative analysis. The composition of the

census data includes 86.33% dicots, 4.83% monocots, 3.27% conifers, 0.71% lycophytes, and 4.86% pteridophytes (Flynn, 2020). This differs from the younger Nacimiento Formation (~64.5-62.1 Ma) that only yielded 39 morphotypes out of 2117 specimens. Further, dicots, monocots, and lycophytes in this study make up a smaller percentage of the counted specimens, while pteridophytes make up over 10% more compared to the older floras in the basin. Additionally, the most prominent species in the Ojo Alamo Formation was *Averrhoites affinis* while in the Nacimiento Formation it was not identified at any of the sites. Interestingly, in addition to documenting fewer total morphotypes, the species richness of the Nacimiento floras, was considerably lower than the Ojo Alamo floras (Figure 3.1). However, the evenness and dominance of the floras from the two formations are similar (Table 3.2). This suggests that while there was a drop in species richness in the basin through time, diversity levels are relatively similar.

Paleoclimate estimates of the Ojo Alamo floras indicate a seasonal tropical forest biome with a pronounced dry season, with MAT ranging from $23.5 \pm 2.5^{\circ}\text{C}$ (using LMA) to $27.4 \pm 4.0^{\circ}\text{C}$ (using DiLP) (Flynn, 2020). These MAT reconstructions are almost ten degrees warmer than the younger floras of the Nacimiento record, indicating a significant cooling trend through time (Figure 4.1). This decrease in temperature may have driven the decrease in species richness through time as taxa adapted to warmer conditions dispersed out of the basin or went extinct. MAP of the two formations are similar, so precipitation levels appear to be relatively constant through time. However, it is important to note the Flynn (2020) suggested the MAP may be underestimated for the Ojo Alamo Formation, which if correct, would suggest the MAP may have also decrease through time.

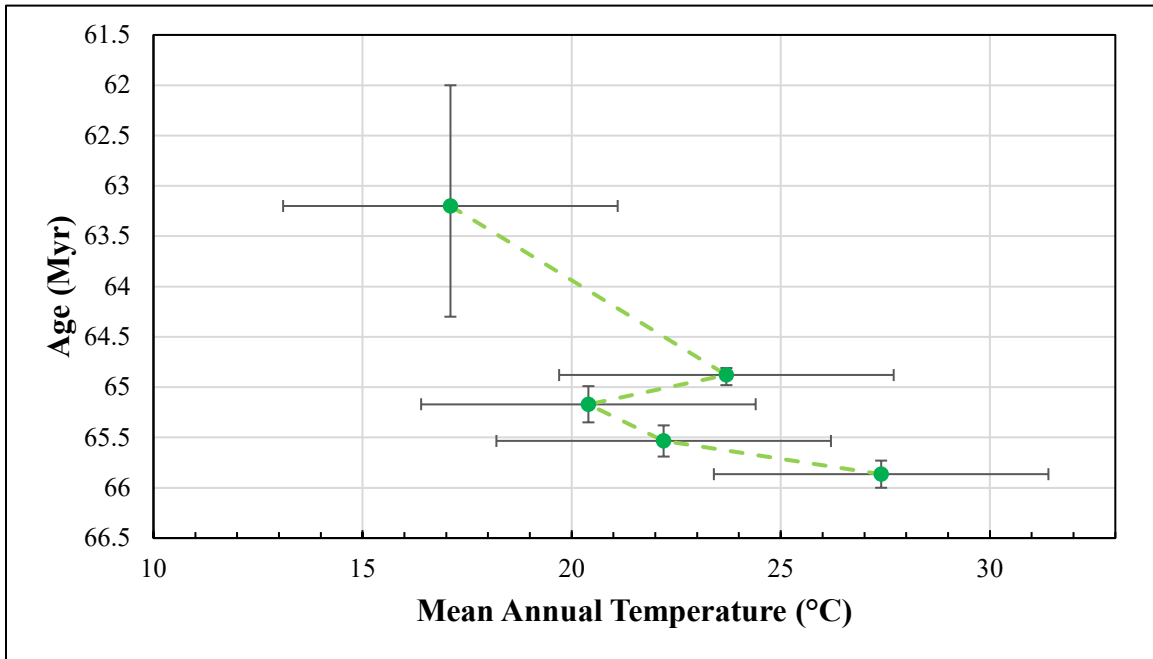


Figure 4.1. DiLP temperature estimates through time in the San Juan Basin.

Regional Patterns of Floral Composition, Diversity, and Paleoclimate

With the further addition of floral records from the San Juan Basin, regional patterns and trends in composition of Paleocene floras can be examined. Comparisons of diversity of floras from the Northern Great Plains basins (e.g. Hanna, Williston, Denver, Bighorn), show that there is a large drop in species richness across the K-Pg boundary and that diversity levels remain low through much of the Paleocene (Hickey, 1980; Johnson 2002; Barclay et al., 2003; Dunn, 2003; Peppe, 2010), though there are important exemptions (e.g., the Castle Rock flora of the Denver Basin, Johnson et al., 2002). Interestingly, the earliest Paleocene floras in the San Juan Basin have considerably higher species richness (10-55% higher) than other contemporaneous North American floras (Flynn, 2020). Additionally, the floras are ~15-20% higher in rarefied richness at site level and ~35-40% higher rarefied richness at a basin level (Flynn, 2020). While the

floras in the SJB have higher species richness than the other basins, the plant communities tend to be less even and dominated by common taxa (Flynn, 2020). While the SJB records higher species richness in the early Paleocene compared to other basins, floral communities examined in this study indicate that site level species richness drops to a similar level recorded in the Hanna, Williston, and Denver basins in the middle Paleocene (see Figure 3.1).

Mean annual temperature (MAT) was calculated from leaf margin analysis (LMA) at all basins. Another climatic variable, mean annual precipitation (MAP), was reconstructed in the Hanna and Denver basins. In the WB, floral records indicate a small decrease in MAT into the middle Paleocene from $10.24 \pm 2.97^{\circ}\text{C}$ to $8.18 \pm 2.66^{\circ}\text{C}$ (Peppe, 2010). The work done by Hickey in the BB shows a decrease in MAT through the Puercan, steady MATs of 10°C from the end of the Puercan through the Tiffanian, followed by a slight increase in MAT to 13.5°C during the Clarkforkian (1980). In the Hanna basin, MAT values are consistent besides a slight cooling event in the Torrejonian; MAT values were at $22.4 \pm 2.9^{\circ}\text{C}$ then decreased to $14.9 \pm 3.9^{\circ}\text{C}$ and $16.4 \pm 4.4^{\circ}\text{C}$. MAP was also calculated in the HB, showing values of 87-179 cm/year (Dunn, 2003). Within the DB, MAT was calculated to be $18.6 \pm 2.6^{\circ}\text{C}$ and MAP had a range of 152-305 cm/year (Barclay et al., 2003). This drop in temperature through the early and middle Paleocene appears to be recorded in all of the major Great Plains basins and in the SJB (see Figure 4.1).

This study has furthered the North American floral record which has allowed us to analyze regional patterns of Paleocene floral communities and paleoclimate. Our results of decreasing diversity and cooling through the Paleocene mirror the results

observed in the BB, WB, and HB, suggesting there is a large scale regional climatic control that is driving the drop in species richness.

CHAPTER FIVE

Conclusions

The fossil flora of the Nacimiento Formation in the San Juan Basin is comprised of 39 distinct morphotypes. The flora was dominated by dicot angiosperms with lycophytes, monocots, and pteridophytes comprising the accessory species. Diversity analyses indicate that there was a drop in species richness while diversity levels are maintained, with the exception of site DG2104 which was heavily dominated by one morphotype due to the facies effect. Mean annual temperature is constant throughout the section within this study but shows an overall decrease in temperature from the start of the earliest Paleocene. Paleoclimate estimates from the fossils indicate the basin is comparable to a modern temperate forest to rainforest to tropical seasonal forest with seasonal variation in precipitation. While species richness is generally higher within the older fossil flora of the SJB, the same patterns are observed in the basin as are in the Northern Great Plains basins. Through the Paleocene, the basins experience a drop in temperature and a subsequent drop in species richness indicating there is a large, regional control on climate and diversity. With the expansion of the floral records in the San Juan Basin, larger overarching patterns are more readily observed latitudinally across North America as well as temporally throughout the basin. This has allowed for further understanding of how plant communities adapt and evolve to changes in climate and whether these changes occur as part of a larger pattern.

APPENDIX

APPENDIX

Supplemental Data and Morphotype Descriptions

This appendix consists of the raw census data, the raw data used for digital leaf physiognomy, and descriptions and images for each morphotype described in localities DG2102, DG2104, DG2109, and DG2110. Dicotyledonous angiosperm (dicot) leaves were described using the Manual of Leaf Architecture (Ellis et al., 2009). Based on the features observed when describing the fossil floras, the fossils were placed into unique morphotypes (Ellis et al., 2009; Peppe et al., 2008).

Each morphotype is represented by a description of the leaf architecture followed by images of the morphotype with a figure caption listing the localities at which the morphotype was identified and the specimen labels. All scale bars are four centimeters long. Dicots are listed first, followed by monocots, pteridophytes, lycopods, and seeds. All fossils from this study are housed at Baylor University Department of Geosciences in the Terrestrial Paleoclimatology and Paleobotany Research Lab.

Table A.1. Raw census data for all studied sites.

<i>SJB</i>	Census Data	
	<i>Number of Specimens</i>	<i>Toothed (T) or Entire (E)</i>
5	9	E
9	2	T
11	45	E
16	78	T
27	116	T
28	203	E
35	4	E
36	15	T
38	24	T
40	149	T
57	54	N/A
64	20	N/A
70	1	N/A
80	26	E
81	37	E
86	73	N/A
95	2	N/A
101	1	N/A
105	281	E
106	18	E
107	7	T
115	15	N/A
116	19	N/A
117	3	N/A
127	2	T
137	10	E
148	2	N/A
157	7	E
158	208	N/A
192	2	N/A
500	545	T
501	2	E
502	82	T
503	1	E
505	2	E
506	2	E
507	11	E
508	17	E
509	22	E

Table A.2. Raw DiLP data.

Locality	Morphotype	Specimen #	Margin	Petiole Width (cm)	Petiole Area (cm ²)	Inferred Blade Area (cm ²)	Raw Blade Area (cm ²)	Raw Perimeter (cm)	Major Length (cm)	Length of Cut Perimeter (cm)	Raw Internal Perimeter (cm)	Raw Internal Blade Area (cm ²)	# 1° Teeth	# 2° Teeth	Tooth Area (cm ²)
DG2102-C	SJ-105	DG2102-C-39	E	0.6		37.84		25.32	11.38						
DG2102-C	SJ-105	DG2102-C-46	E	0.11		27.9		23.05	8.68						
DG2102-C	SJ-105	DG2102-C-45	E	0.34	0.18	15.52		15.66	5.59						
DG2102-C	SJ-506	DG2102-C-30/43	E	0.21	0.02			26.99	10.59						
DG2102-C	SJ-25	DG2102-C-27/25	E	0.1				55.7	17.13						
DG2102-C	SJ-11	DG2102-C-54B	E	0.22	0.11	65.68		67.36	15.63						
DG2102-C	SJ-27	DG2102-C-63	T	0.15	0.11	90.16	23.3	20.12	14.58	9.72	19.8	23.12	5	0	0.18
DG2102-C	SJ-11	DG2102-C-54	E	0.28		71.74		55.5	16.3						
DG2104	SJ500	DG2104-27	T	0.051			2.388	6.566		3.374	6.413	2.369	4		0.019
DG2104	SJ500	DG2104-voucher	T	0.063			8.955	13.031		8.618	12.339	8.749	5.5		0.206
DG2104	SJ500	DG2104-voucher	T	0.125			26.815	22.753		10.694	21.807	26.291	3	3	0.524
DG2104	SJ507	DG2104-voucher	E	0.042		17.506			6.733						
DG2110	SJ-28	DG2110-C-18	E	0.255		108.096			16.091						

Continued

Locality	Morphotype	Specimen #	Margin	Petiole Width (cm)	Petiole Area (cm ²)	Inferred Blade Area (cm ²)	Raw Blade Area (cm ²)	Raw Perimeter (cm)	Major Length (cm)	Length of Cut Perimeter (cm)	Raw Internal Perimeter (cm)	Raw Internal Blade Area (cm ²)	# 1° Teeth	# 2° Teeth	Tooth Area (cm ²)
DG2110	SJ-28	DG2110-C-31	E	0.18	0.19	33.044			11.09						
DG2110	SJ-28	DG2110-C-41	E	0.163		56.206			13.266						
DG2110	SJ-40	DG2110	T	0.076		41.737	12.266	14.416	8.666	9.708	14.184	12.175	7	0	0.111
DG2110	SJ-80	DG2110-C-1	E	0.079		37.734			11.68						
DG2110	SJ-80	DG2110-C-36	E	0.116		14.444			7.219						
DG2110	SJ-506	DG2110-C-59	E	0.052		5.974			5.504						
DG2110	SJ-508	DG2110-C-9	E	0.019		32.75			10.181						
DG2110	SJ-36	DG2110-C-55	T	0.032			1.509	5.522		3.457	5.252	1.486	2	4	0.023
DG2109	SJ-16	DG2109-C-60	T	0.064			2.783	10.081		4.843	9.778	2.724	2	0	0.059
DG2109	SJ-16	DG2109-C-74	T	0.058			13.899	18.89		10.953	18.031	13.68	12	0	0.219
DG2109	SJ-502	DG2109-C-2	T	0.02			1.846	6.828		3.627	5.86	1.8	8	4	0.046
DG2109	SJ-502	DG2109-C-26	T	0.055			1.671	6.107		3.599	5.643	1.65	10	0	0.021
DG2109	SJ-502	DG2109-C-71	T	0.114	0.012		0.865	4.367		2.194	4.067	0.855	6	0	0.01
DG2109	SJ-506	DG2109-C-75	E	0.057	0.114	6.234			6.148						
DG2109	SJ-40	DG2109-C-81	T	0.102	0.044		2.297	7.17		3.91	6.696	2.249	6	0	0.048

Morphotype SJ-5 Leaf Architecture Description

Laminar shape elliptic with medial symmetrical and base not visible. Primary venation pinnate. Major secondaries eucamptodromous, spacing uniform; attachment decurrent. Intercostal tertiary veins straight opposite percurrent, vein angle consistent. Proximal course perpendicular to midvein; distal course parallel to intercostal tertiary.



Figure A.1. Morphotype SJ-5. Present in locality DG2102. Specimen number: DG2102-C-64.

Morphotype SJ-9 Leaf Architecture Description

Laminar size microphyll; laminar shape elliptic with medial symmetrical. Margin unlobed and serrate. Apex angle acute; base angle acute. Primary venation pinnate; agrophic veins absent. Major secondaries semicraspedodromous, spacing gradually increasing proximally, uniform; attachment decurrent. Intercostal tertiary veins opposite percurrent; obtuse to midvein. Epimedial tertiaries opposite percurrent; proximal course perpendicular to midvein; distal course parallel to intercostal tertiary. Tooth spacing irregular, with two orders of teeth; teeth / cm 6; sinus shape rounded. Tooth shapes rt/st; st/cv; and rt/cv.

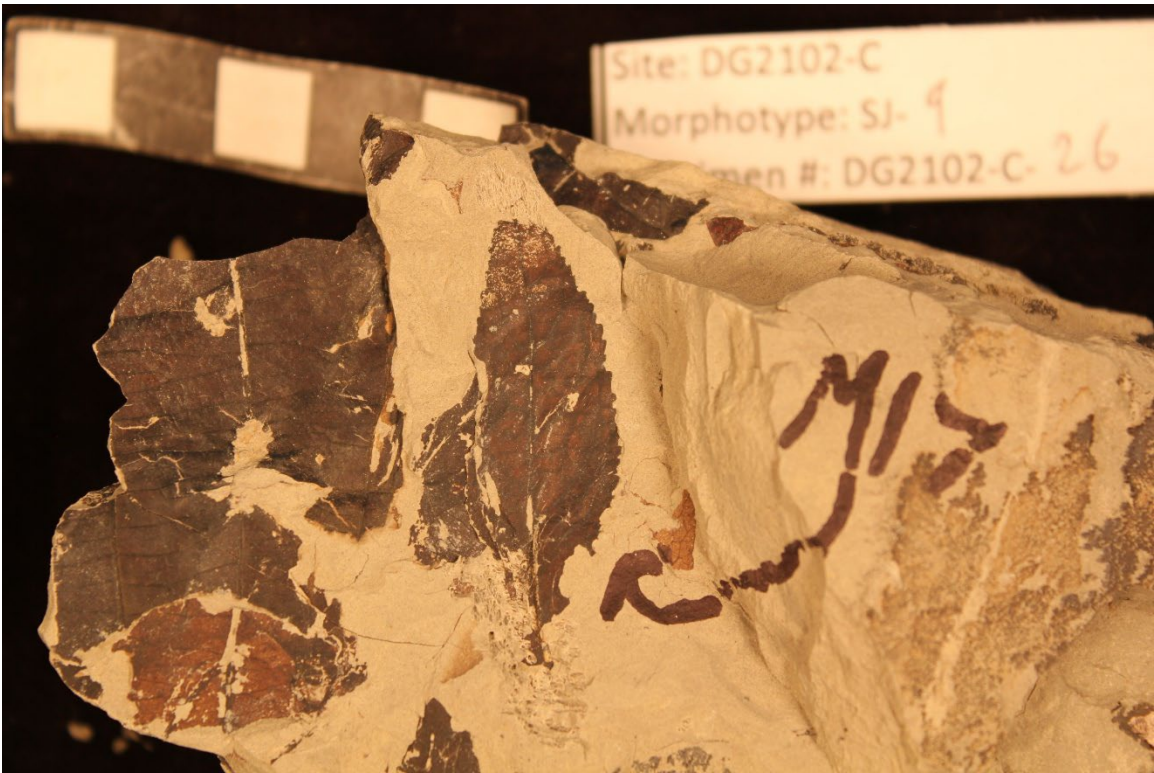


Figure A.2. Morphotype SJ-9. Present in locality DG2102. Specimen number: DG2102-C-26.

Morphotype SJ-11 Leaf Architecture Description

Leaf attachment petiolate. Lamina shape elliptic with medial symmetrical and base basal width asymmetrical to symmetrical. Margin unlobed and entire. Apex angle acute; base angle acute; base shape concave to decurrent. Primary venation pinnate. Major secondaries eucamptodromous, spacing regular, smoothly increasing proximally; attachment excurrent. Intercostal tertiary veins opposite percurrent; obtuse to midvein; vein angle not applicable. Epimedial tertiaries opposite percurrent; proximal course perpendicular to midvein; distal course parallel to intercostal tertiary.

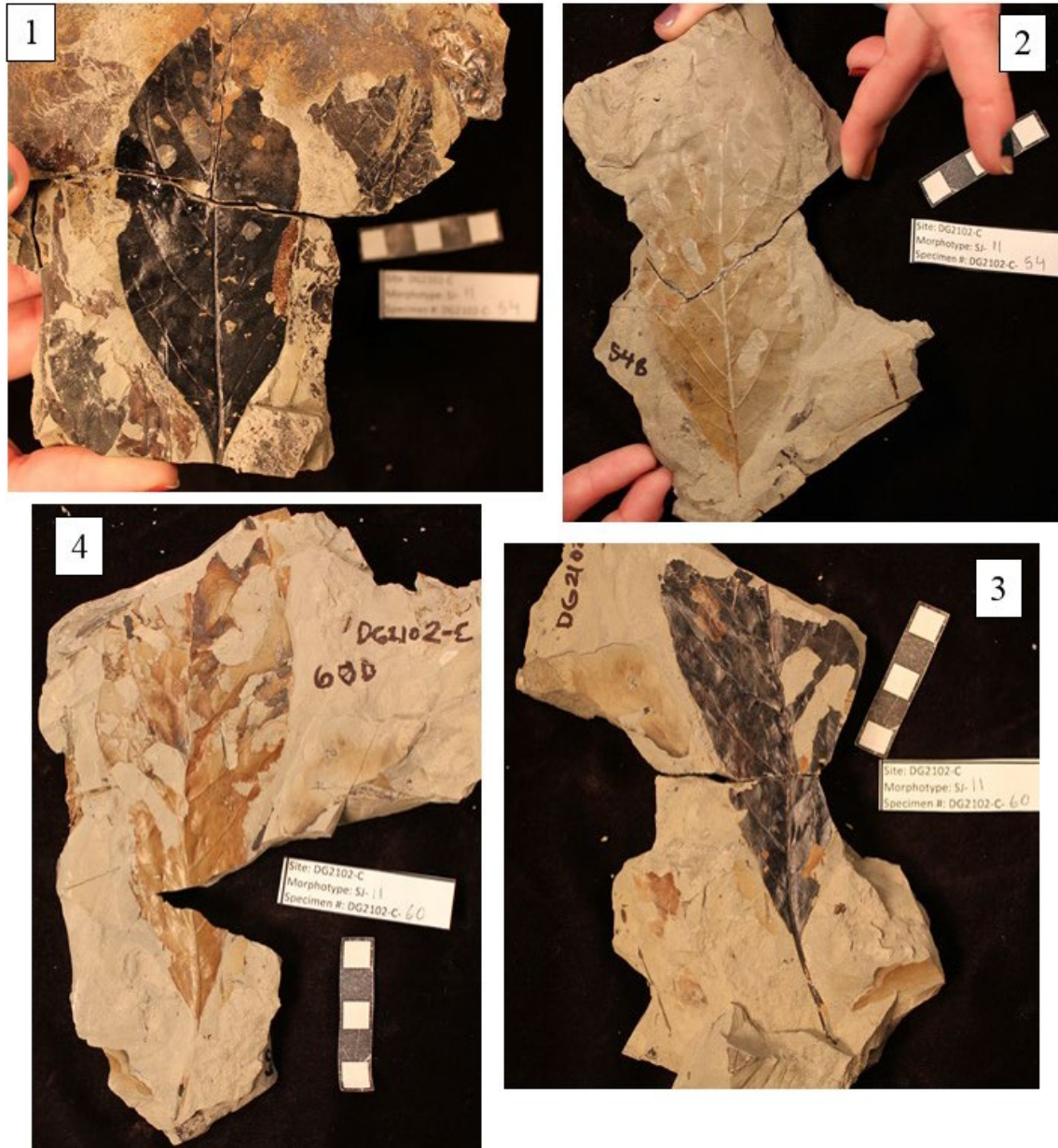


Figure A.3. Morphotype SJ-11. Present in localities DG2102, DG2109, and DG2110. Specimen number: 1. DG2102-C-54, 2. DG2102-C-54.1, 3. DG2102-C-60, 4. DG2102-C-60.

Morphotype SJ-16 Leaf Architecture Description

Leaf attachment petiolate. Blade attachment marginal. Lamina shape obovate with medial symmetrical and base symmetrical. Margin palmately lobed and dentate. Apex angle acute; apex shape straight; base angle acute; base shape concave. Primary venation suprabasal acrodromous. Major secondaries craspedodromous, spacing regular, uniform; attachment excurrent. Intercostal tertiary veins convex opposite percurrent; acute to midvein; vein angle consistent. Epimedial tertiaries opposite percurrent; proximal course perpendicular to midvein; distal course parallel to intercostal tertiary. Quaternary vein fabric alternate percurrent. Tooth spacing regular, with one order of teeth; teeth / cm 4; sinus shape rounded. Tooth shapes rt/cc; cv/st; and cc/cc. Principal vein present; terminates at tooth apex.

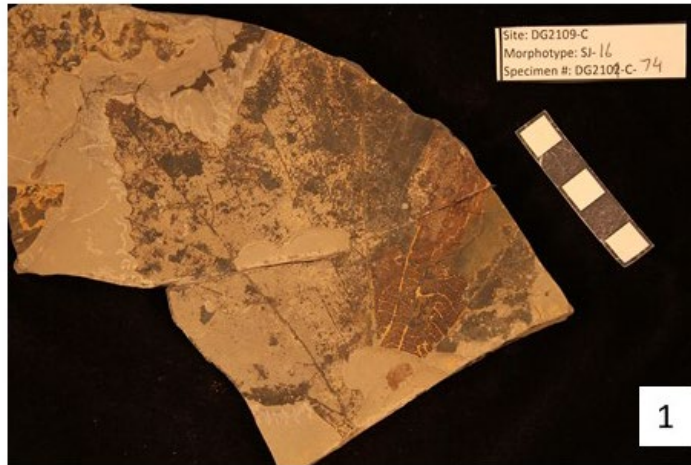


Figure A.4. Morphotype SJ-16. Present in locality DG2109. Specimen number: 1. DG2109-C-74, 2. DG2109-C-60, 3. DG2109-C-51.

Morphotype SJ-27 Leaf Architecture Description

Leaf attachment petiolate. Blade attachment peltate excentric. Margin serrate. Base angle circular; base shape rounded. Primary venation basal actinodromous; agrophic veins present. Major secondaries craspedodromous, spacing regular, uniform; attachment excurrent. Intercostal tertiary veins convex opposite percurrent; perpendicular to midvein; vein angle consistent. Epimedial tertiaries opposite percurrent; proximal course perpendicular to midvein; distal course basiflexed. Quaternary vein fabric opposite percurrent. Quinternary vein fabric regular reticulate. Tooth spacing regular, with two orders of teeth; teeth / cm 2; sinus shape rounded. Tooth shapes cc/cc.

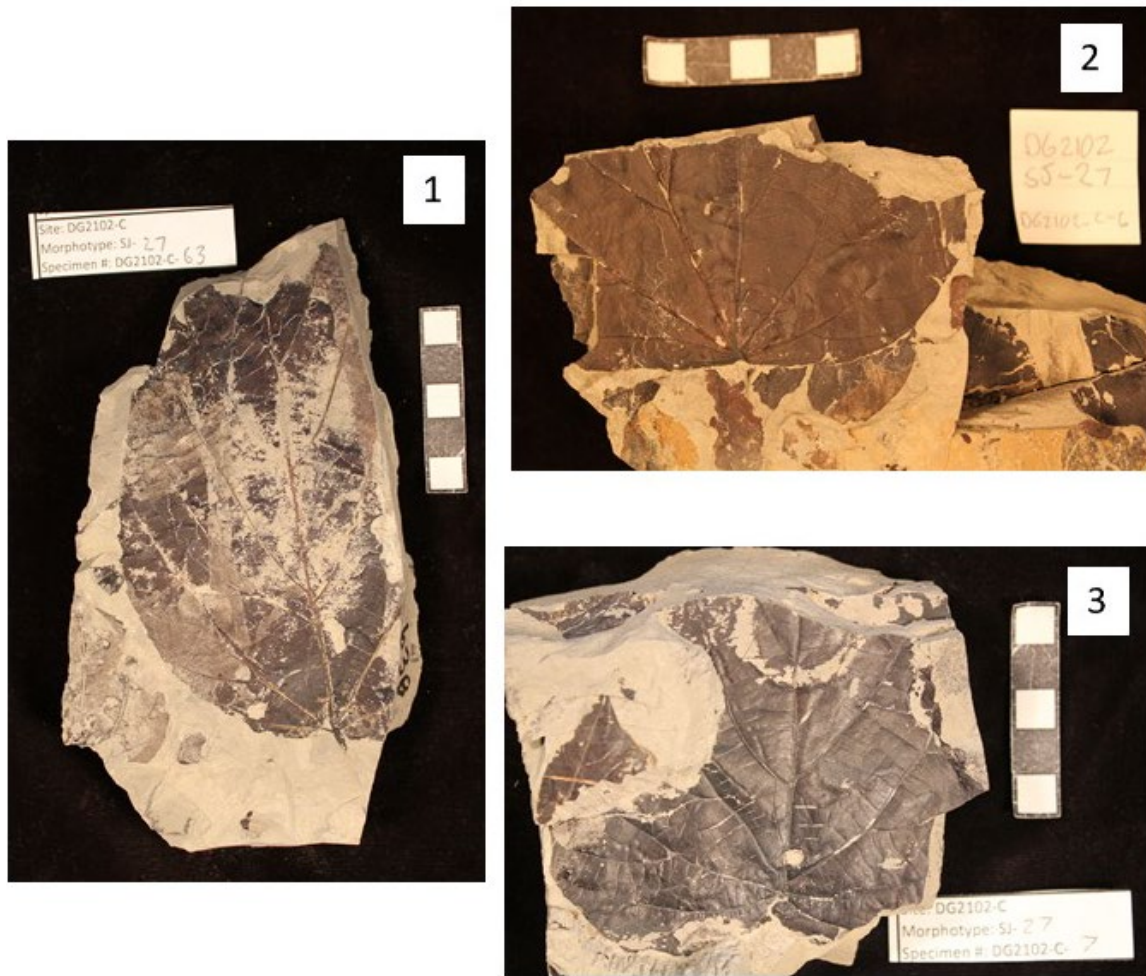


Figure A.5. Morphotype SJ-27. Present in localities DG2102 and DG2104. Specimen number: 1. DG2109-C-63, 2. DG2102-C-6, 3. DG2102-C-7.

Morphotype SJ-28 Leaf Architecture Description

Leaf attachment petiolate. Blade attachment marginal. Margin unlobed and entire. Base angle obtuse; base shape convex. Primary venation pinnate. Major secondaries simple brochidodromous, spacing decreasing proximally, smoothly increasing proximally; attachment excurrent. Intercostal tertiary veins chevroned opposite percurrent; obtuse to midvein; vein angle consistent.

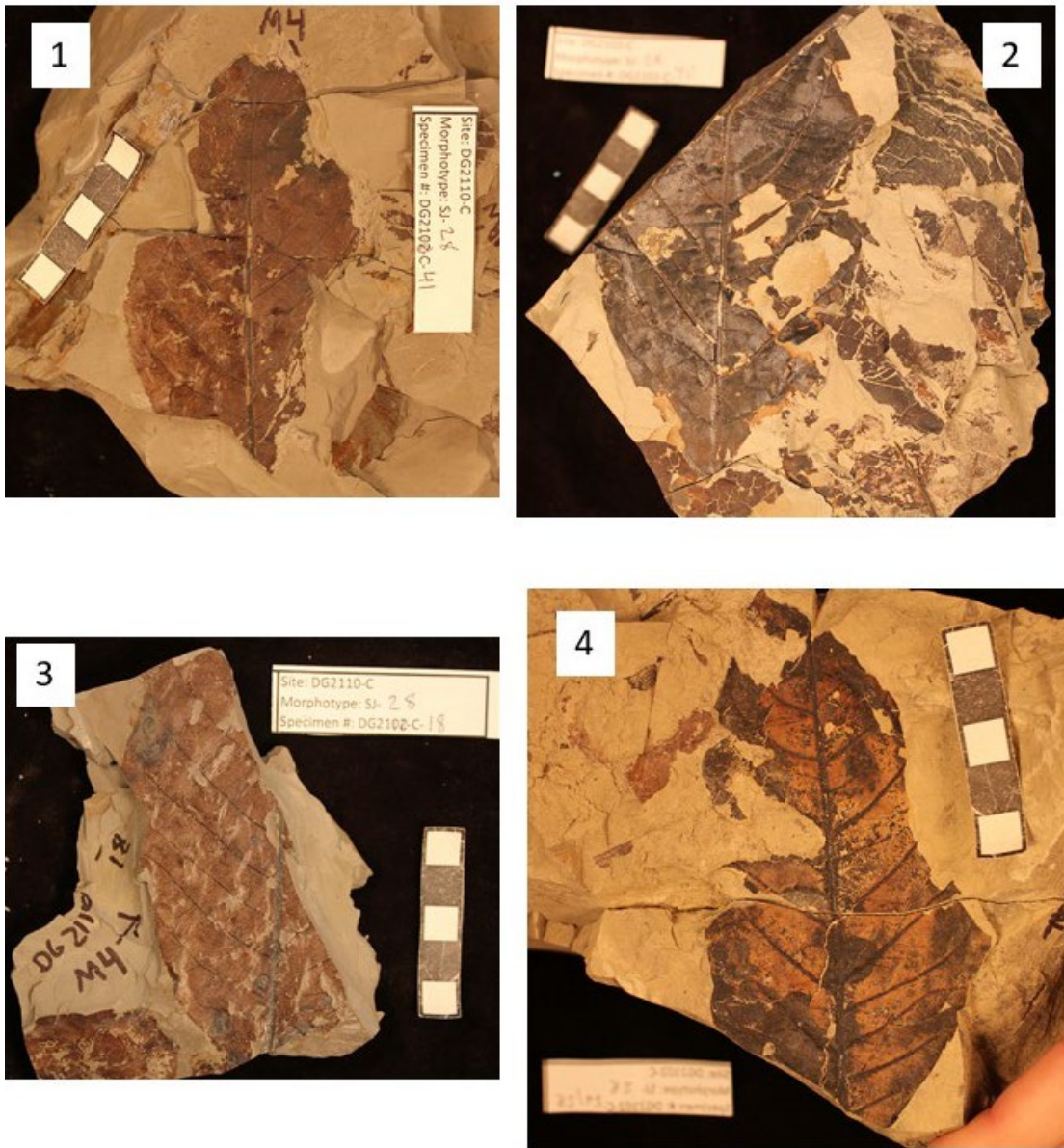


Figure A.6. Morphotype SJ-28. Present in localities DG2102, DG2109, and DG2110. Specimen number: 1. DG2110-C-41, 2. DG2102-C-40, 3. DG2110-C-18, 4. DG2102-C-29.

Morphotype SJ-35 Leaf Architecture Description

Laminar size microphyll; laminar shape ovate with medial asymmetrical. Margin unlobed and entire. Apex angle acute Primary venation pinnate. Major secondaries simple brochidodromous, spacing gradually increasing proximally, uniform; attachment excurrent. Intercostal tertiary veins sinuous opposite percurrent; acute to midvein. Epimedial tertiaries proximal course perpendicular to midvein; distal course parallel to intercostal tertiary.



Figure A.7. Morphotype SJ-35. Present in locality DG2104. Specimen number: 1. DG2104-C-33, 2. DG2104-C-36.

Morphotype SJ-36 Leaf Architecture Description

Laminar shape ovate. Margin dentate. Primary venation pinnate. Major secondaries craspedodromous, spacing regular, uniform; attachment excurrent. Intercostal tertiary veins alternate percurrent; obtuse to midvein; vein angle consistent. Epimedial tertiaries proximal course perpendicular to midvein; distal course parallel to intercostal tertiary. Tooth spacing regular, with two orders of teeth; teeth / cm 3; sinus shape rounded. Tooth shapes cc/st; cc/cv; and rt/st. Principal vein present; terminates at apex of tooth.

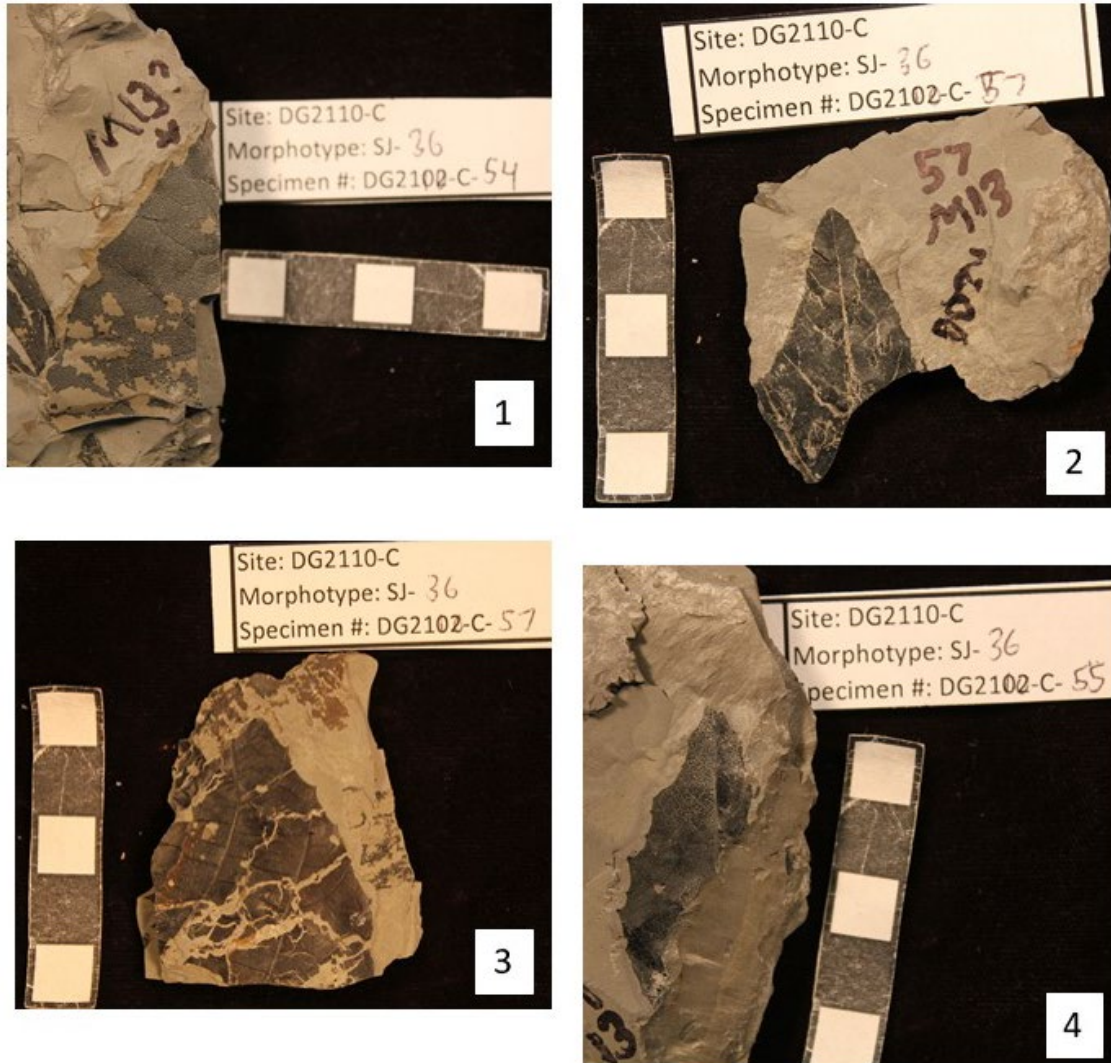


Figure A.8. Morphotype SJ-36. Present in locality DG2110. Specimen number: 1. DG2110-C-54, 2. DG2110-C-57, 3. DG2110-C-57.1, 4. DG2110-C-55.

Morphotype SJ-38 Leaf Architecture Description

Laminar shape ovate with medial symmetrical and base symmetrical. Margin unlobed and entire. Primary venation pinnate. Major secondaries craspedodromous, spacing gradually increasing proximally, smoothly increasing proximally; attachment excurrent.

Intercostal tertiary veins straight opposite percurrent; obtuse to midvein; vein angle decreasing proximally. Epimedial tertiaries proximal course perpendicular to midvein; distal course parallel to intercostal tertiary. Quaternary vein fabric alternate percurrent.

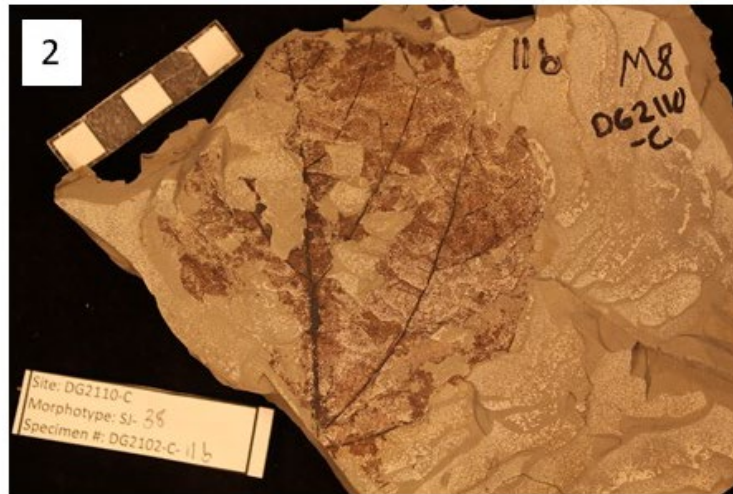


Figure A.9. Morphotype SJ-38. Present in locality DG2110. Specimen number: 1. DG2110-C-22, 2. DG2110-C-11b, 3. DG2110-C-53, 4. DG2110-C-50.

Morphotype SJ-40 Leaf Architecture Description

Leaf attachment petiolate. Blade attachment marginal. Lamina shape obovate with medial symmetrical and base symmetrical. Margin unlobed and serrate. Apex angle acute; apex shape acuminate; base angle obtuse; base shape truncate to concavo-convex. Primary venation pinnate; agrophic veins present. Major secondaries craspedodromous, spacing gradually increasing proximally, uniform; attachment excurrent. Interior secondaries minor secondary course craspedodromous. Intercostal tertiary veins sinuous opposite percurrent; obtuse to midvein; vein angle consistent. Epimedial tertiaries proximal course perpendicular to midvein; distal course parallel to intercostal tertiary. Quaternary vein fabric alternate percurrent. Tooth spacing regular, with three orders of teeth; teeth / cm 4; sinus shape rounded. Tooth shapes cc/st; and cc/cc. Principal vein present; terminates at the apex of the tooth.

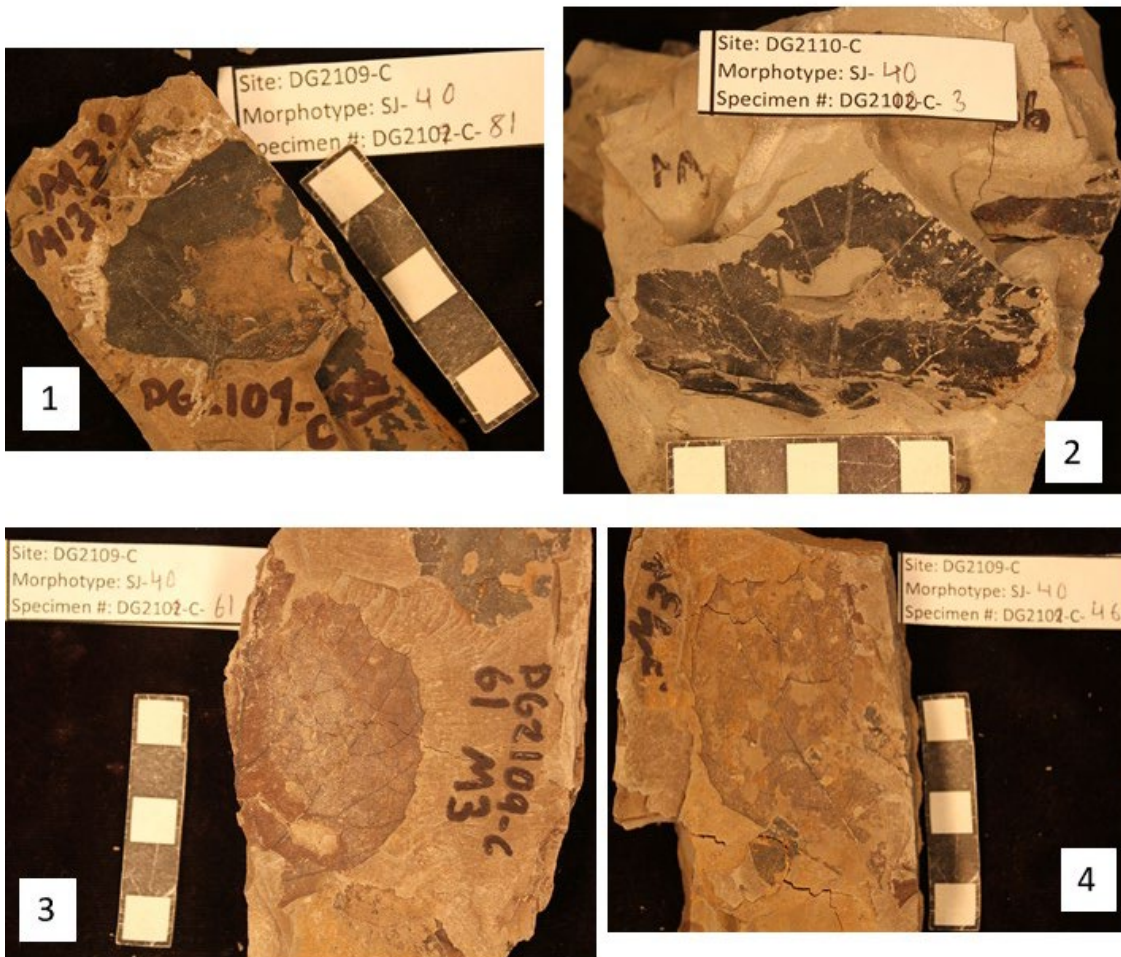


Figure A.10. Morphotype SJ-40. Present in localities DG2109 and DG2110. Specimen number: 1. DG2109-C-81, 2. DG2109-C-3, 3. DG2109-C-61, 4. DG2109-C-46.

Morphotype SJ-80 Leaf Architecture Description

Laminar size microphyll; laminar L:W ratio 3:1; laminar shape oblong with medial symmetrical. Margin unlobed and entire. Apex angle acute; apex shape straight visible.

Primary venation pinnate. Major secondaries eucamptodromous becoming brochidodromous distally, spacing regular, uniform; attachment excurrent. Intercostal tertiary veins straight opposite percurrent to sinuous opposite percurrent; obtuse to midvein; vein angle decreasing exmedially. Epimedial tertiaries opposite percurrent; proximal course perpendicular to midvein; distal course parallel to intercostal tertiary.

Exterior tertiary course looped. Quaternary vein fabric alternate percurrent.



Figure A.11. Morphotype SJ-80. Present in localities DG2109 and DG2110. Specimen number: 1. DG2110-C-1, 2. DG2109-C-65, 3. DG2110-C-x, 4. DG2110-C-30.

Morphotype SJ-81 Leaf Architecture Description

Leaf attachment petiolate. Blade attachment marginal. Laminar shape elliptic with medial symmetrical and base symmetrical. Margin unlobed and entire. Apex angle acute; apex shape acuminate; base angle acute; base shape convex. Primary venation pinnate. Major secondaries simple brochidodromous, spacing regular; attachment excurrent. Intercostal tertiary veins straight opposite percurrent to alternate percurrent; obtuse to midvein; vein angle increasing proximally.



Figure A.12. Morphotype SJ-81. Present in locality DG2110. Specimen number: 1. DG2110-C-13, 2. DG2110-C-2.

Morphotype SJ-105 Leaf Architecture Description

Leaf attachment petiolate. Blade attachment marginal. Laminar shape ovate with medial symmetrical and base symmetrical. Margin unlobed and entire. Apex angle acute; apex shape straight; base angle obtuse; base shape truncate to rounded. Primary venation pinnate; agrophic veins present. Major secondaries simple brochidodromous, spacing abruptly increasing proximally, uniform; attachment excurrent. Minor secondary course simple brochidodromous. Intercostal tertiary veins straight opposite percurrent to convex opposite percurrent; obtuse to midvein; vein angle consistent. Epimedial tertiaries proximal course perpendicular to midvein; distal course parallel to intercostal tertiary. Quaternary vein fabric alternate percurrent.

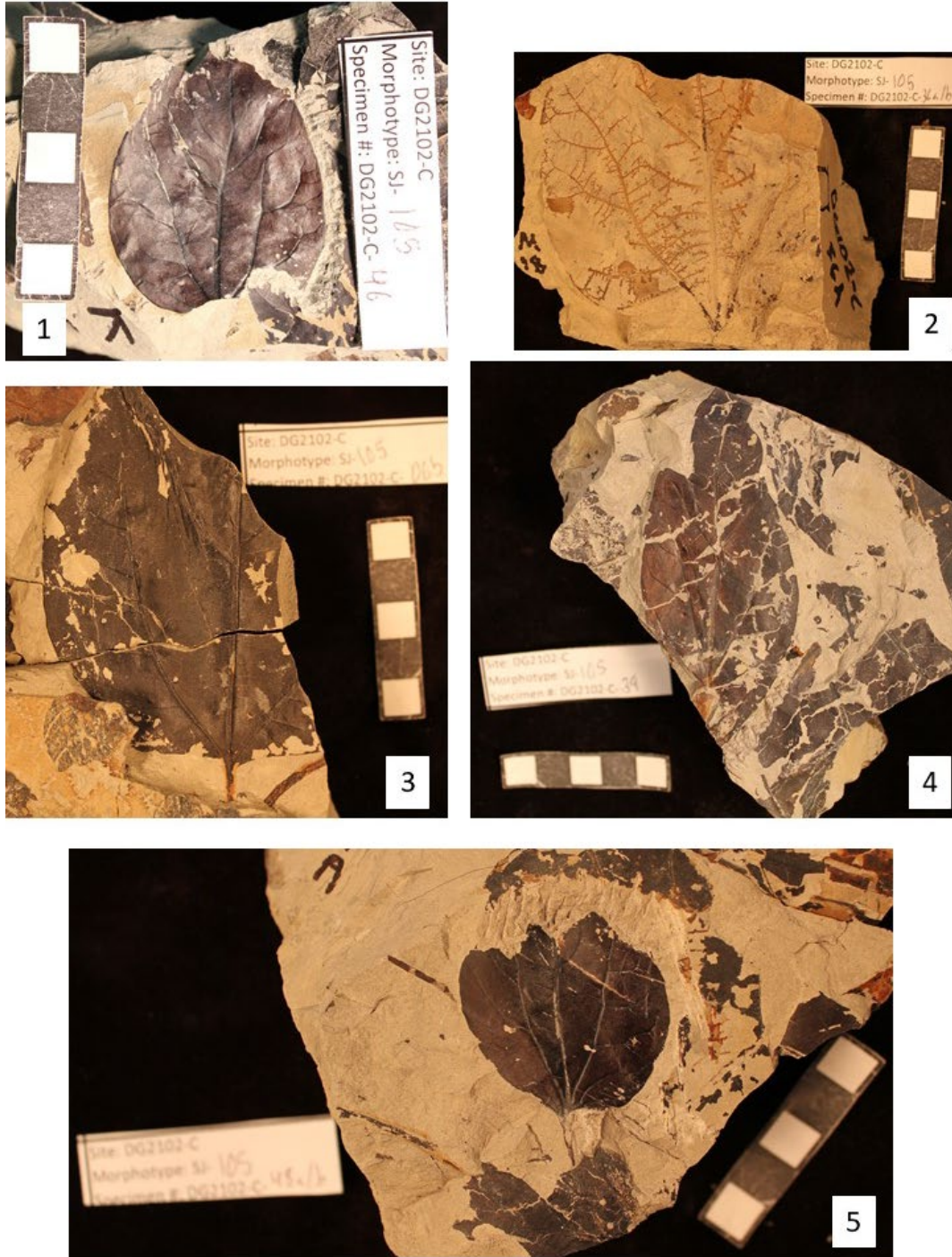


Figure A.13. Morphotype SJ-105. Present in localities DG2102 and DG2110. Specimen number: 1. DG2102-C-46, 2. DG2102-C-36, 3. DG2102-C-65, 4. DG2102-C-39, 5. DG2102-C-48.

Morphotype SJ-106 Leaf Architecture Description

Leaf attachment petiolate. Margin unlobed and entire. Base angle reflex; base shape concavo-convex. Primary venation basal actinodromous. Major secondaries decurrent. Intercostal tertiary veins chevroned opposite percurrent to sinuous opposite percurrent; acute to midvein; vein angle consistent. Epimedial tertiaries proximal course acute to midvein; distal course parallel to intercostal tertiary. Quaternary vein fabric alternate percurrent.



Figure A.14. Morphotype SJ-106. Present in locality DG2102. Specimen number: 1. DG2102-C-66, 2. DG2102-C-15.

Morphotype SJ-107 Leaf Architecture Description

Laminar shape ovate with medial symmetrical. Margin unlobed and serrate. Apex angle acute; apex shape acuminate. Terminal apex mucronate. Primary venation pinnate. Major secondaries craspedodromous, spacing decreasing proximally, uniform; attachment excurrent. Intercostal tertiary veins straight opposite percurrent. Tooth spacing regular, with two orders of teeth; teeth / cm 2; sinus shape angular. Tooth shapes cc/st; cv/st; and cv/cc. Principal vein present; terminates at tooth apex.



Figure A.15. Morphotype SJ-107. Present in locality DG2104. Specimen number: 1. DG2104-C-29, 2. DG2104-C-35.

Morphotype SJ-127 Leaf Architecture Description

Laminar shape elliptic. Margin unlobed and serrate. Apex angle acute; apex shape straight to acuminate. Primary venation pinnate. Major secondaries craspedodromous, spacing gradually increasing proximally, uniform; attachment excurrent. Intercostal tertiary veins straight opposite percurrent, to mixed percurrent; obtuse to midvein; vein angle decreasing exmedially. Epimedial tertiaries opposite percurrent; proximal course perpendicular to midvein; distal course parallel to intercostal tertiary. Exterior tertiary course looped. Quaternary vein fabric alternate percurrent. Quinary vein fabric irregular reticulate. Areolation moderate development. Tooth spacing regular, with two orders of teeth; teeth / cm 2; sinus shape rounded. Tooth shapes st/rt; and cc/st. Principal vein present; terminates at apex of tooth.

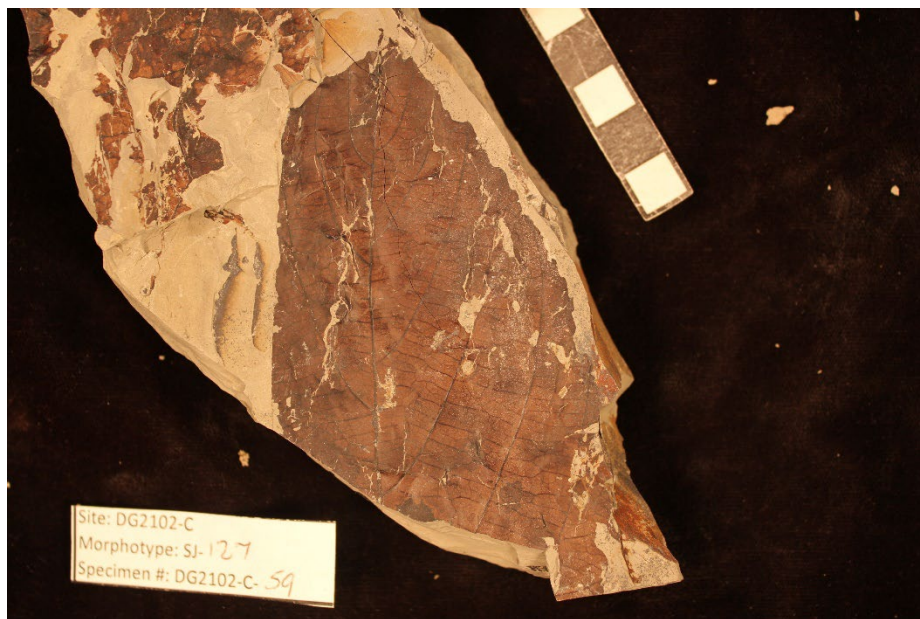


Figure A.16. Morphotype SJ-127. Present in locality DG2102. Specimen number: 1. DG2102-C-59.

Morphotype SJ-137 Leaf Architecture Description

Laminar shape oblong with medial symmetrical. Margin unlobed and entire. Primary venation pinnate. Major secondaries simple brochidodromous, spacing irregular, uniform; attachment excurrent

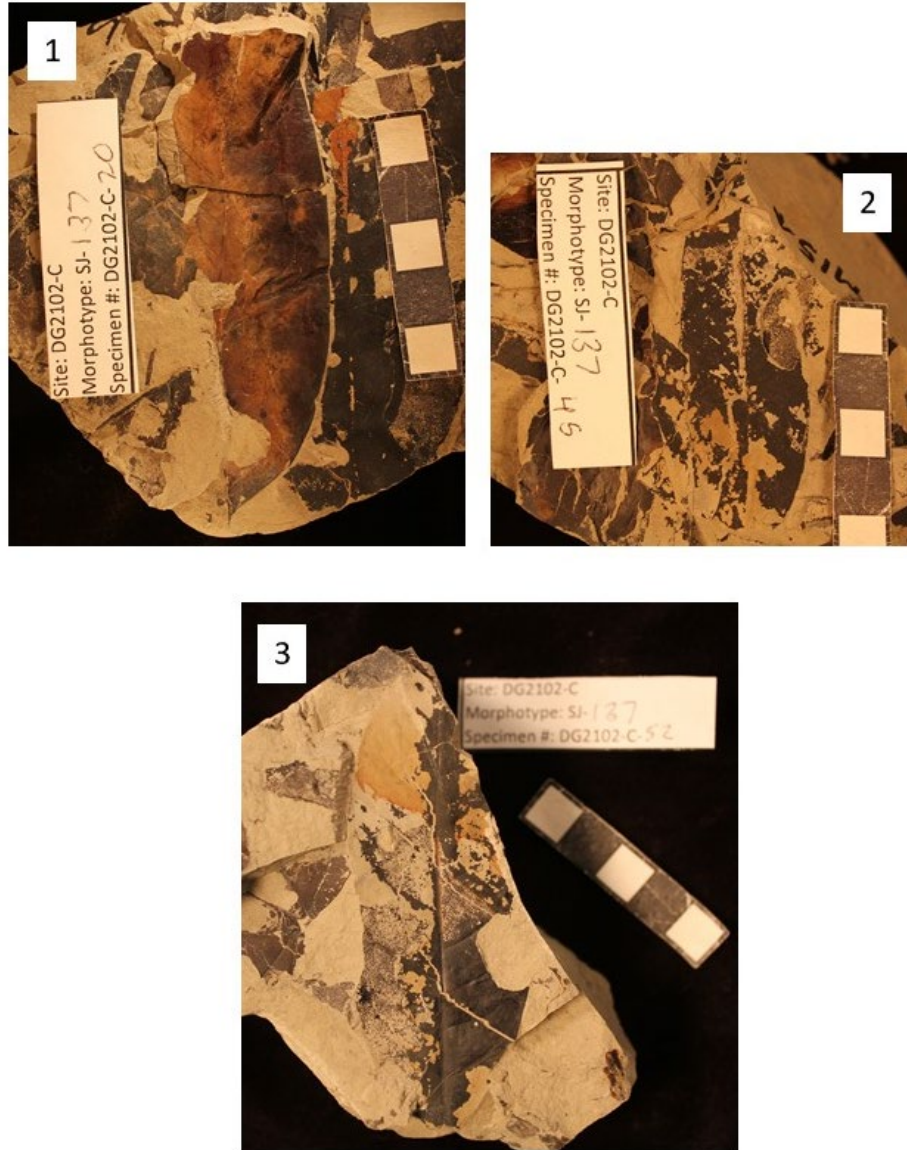


Figure A.17. Morphotype SJ-137. Present in locality DG2102. Specimen number: 1. DG2102-C-20, 2. DG2102-C-45, 3. DG2102-C-52.

Morphotype SJ-157 Leaf Architecture Description

Leaf attachment petiolate. Blade attachment marginal. Laminar size microphyll; laminar shape ovate with medial symmetrical and base symmetrical. Margin entire. Apex angle acute; apex shape straight to acuminate; base angle obtuse; base shape rounded to concave. Primary venation pinnate agrophic veins simple. Major secondaries simple brochidodromous. Intercostal tertiary veins convex opposite percurrent to straight opposite percurrent; obtuse to midvein; vein angle consistent. Epimedial tertiaries opposite percurrent; proximal course perpendicular to midvein; distal course parallel to intercostal tertiary. Exterior tertiary course looped.

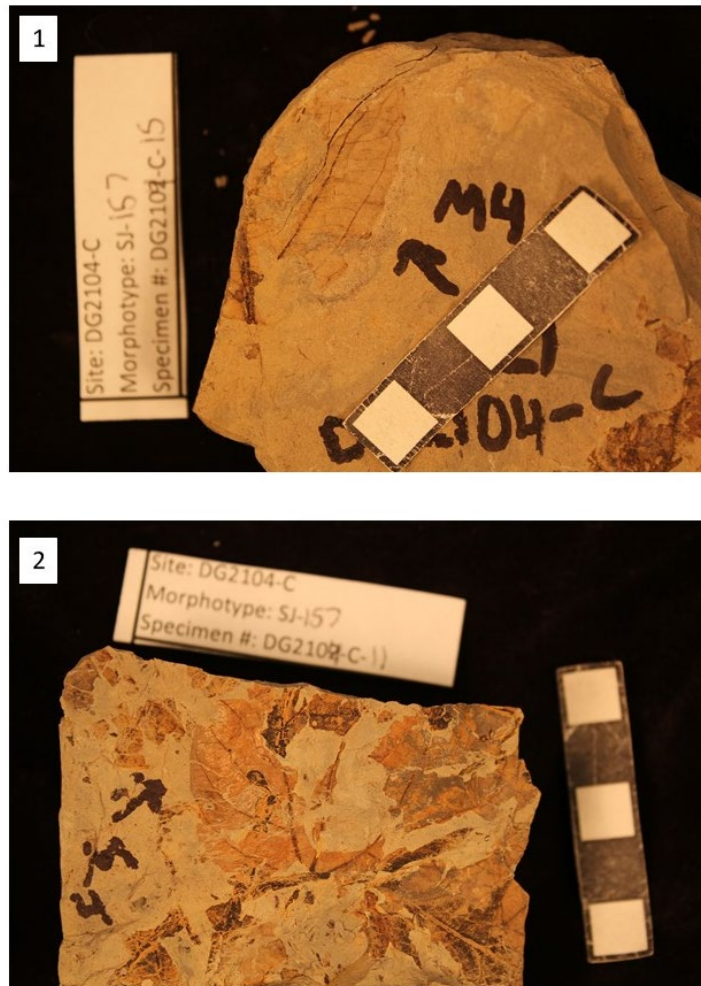


Figure A.18. Morphotype SJ-157. Present in locality DG2104. Specimen number: 1. DG2104-C-15, 2. DG2104-C-11.

Morphotype SJ-500 Leaf Architecture Description

Leaf attachment petiolate. Blade attachment marginal. Laminar shape oblong/ovate with medial symmetrical and base symmetrical. Margin unlobed and serrate. Apex angle acute; base angle obtuse; base shape rounded to convex. Primary venation pinnate; agrophic veins compound. Major secondaries craspedodromous, spacing regular, uniform; attachment excurrent. Interior secondaries absent; minor secondary course simple brochidodromous/craspedodromous. Intercostal tertiary veins chevroned opposite percurrent to sinuous opposite percurrent; obtuse to midvein; vein angle consistent. Epimedial tertiaries opposite percurrent; proximal course perpendicular to midvein; distal course parallel to intercostal tertiary. Exterior tertiary course variable. Tooth spacing regular, with two orders of teeth; teeth / cm ²; sinus shape rounded. Tooth shapes st/rt; cc/cc; and st/st. Principal vein present.

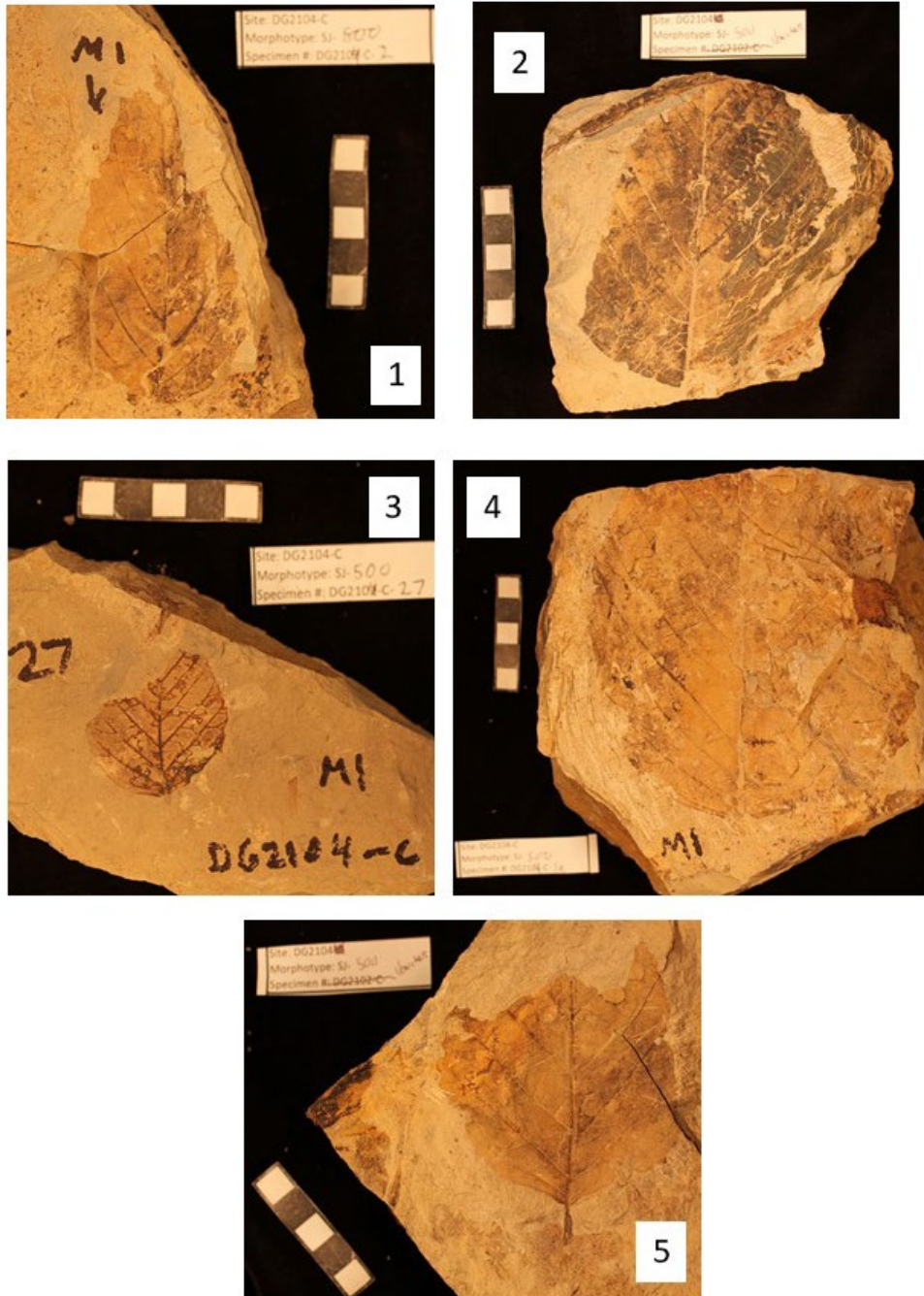


Figure A.19. Morphotype SJ-500. Present in locality DG2104. Specimen number: 1. DG2104-C-2, 2. DG2104-voucher, 3. DG2104-C-27, 4. DG2104-C-19, 5. DG2104-voucher.

Morphotype SJ-501 Leaf Architecture Description

Laminar shape unknown with medial asymmetrical. Margin crenate with sinuous edges. Apex angle acute; apex shape acuminate. Primary venation pinnate. Major secondaries craspedodromous, spacing irregular, inconsistent; attachment excurrent. Intercostal tertiary veins sinuous opposite percurrent; obtuse to midvein; vein angle inconsistent. Tooth spacing irregular, with one order of teeth; teeth / cm 1; sinus shape rounded. Tooth shapes cv/cv; rt/cv; and cv/rt. Principal vein present; terminates present at the apex of the tooth.

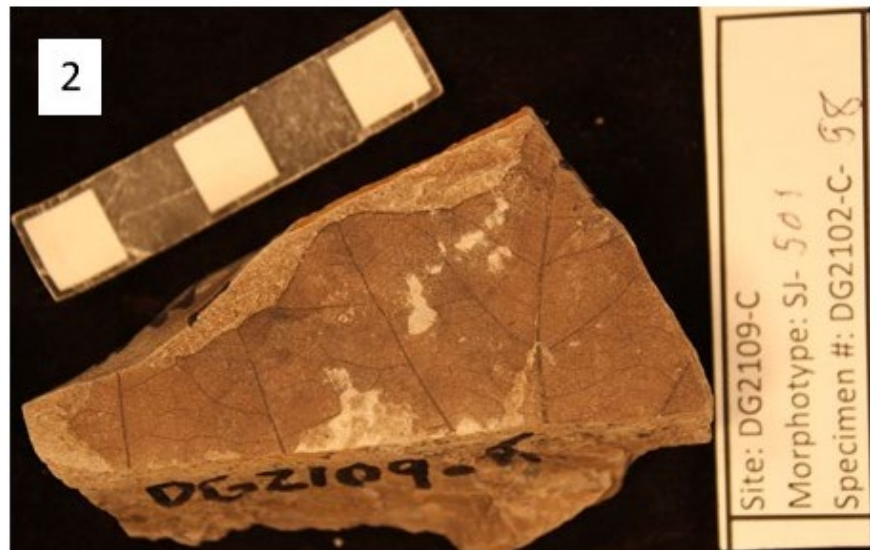
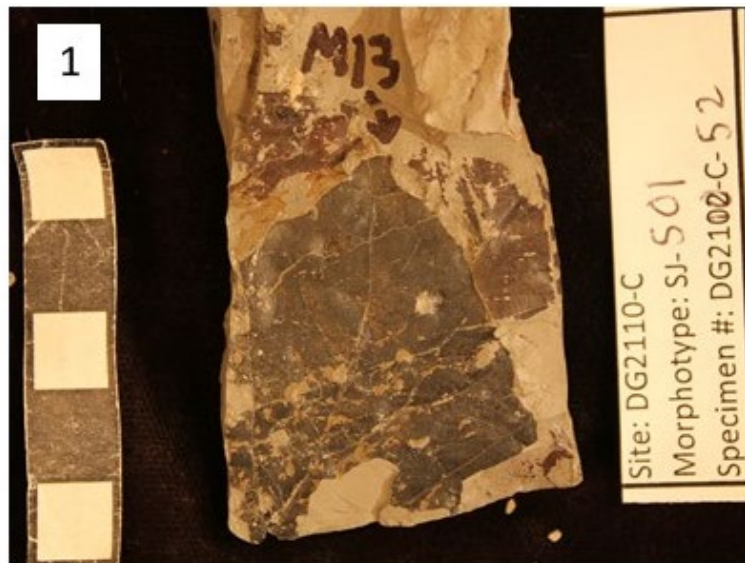


Figure A.20. Morphotype SJ-501. Present in localities DG2109 and DG2110. Specimen number: 1. DG2110-C-52, 2. DG2109-C-58.

Morphotype SJ-502 Leaf Architecture Description

Laminar size microphyll; laminar shape ovate with medial symmetrical and base symmetrical. Margin unlobed and serrate. Apex angle acute; apex shape straight; base angle obtuse; base shape rounded to convex. Primary venation pinnate. Major secondaries semicraspedodromous, spacing regular, uniform; attachment excurrent. Intercostal tertiary veins sinuous opposite percurrent to straight opposite percurrent; obtuse to midvein. Tooth spacing regular, with one order of teeth; teeth / cm 4; sinus shape rounded. Tooth shapes cc/rt. Principal vein present; terminates at apex of the tooth.

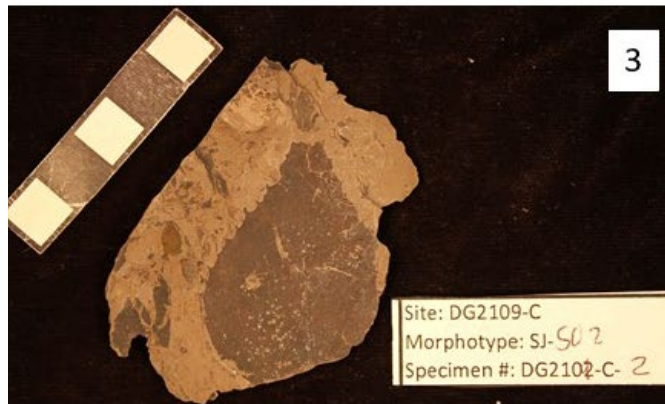


Figure A.21. Morphotype SJ-502. Present in locality DG2109. Specimen number: 1. DG2109-C-71, 2. DG2109-C-26, 3. DG2109-C-2.

Morphotype SJ-503 Leaf Architecture Description

Laminar shape oblong with medial symmetrical. Margin entire. Apex angle acute; apex shape acuminate with drip tip. Primary venation pinnate. Major secondaries attachment excurrent.



Figure A.22. Morphotype SJ-503. Present in locality DG2109. Specimen number: 1. DG2109-C-44, 2. DG2109-C-44.

Morphotype SJ-505 Leaf Architecture Description

Margin lobed and serrate. Teeth / cm 1; sinus shape rounded. Tooth shape cc/st. A partial specimen that appears to be lobed, unable to identify venation.

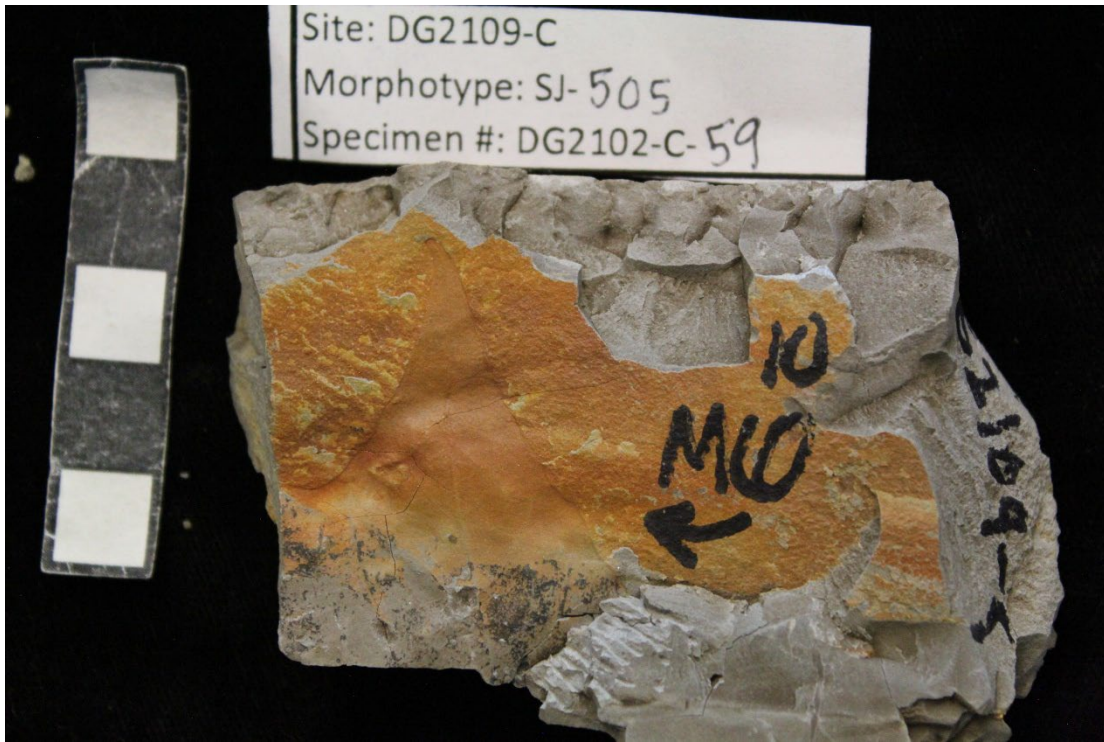


Figure A.23. Morphotype SJ-505. Present in locality DG2109. Specimen number: DG2109-C-59.

Morphotype SJ-506 Leaf Architecture Description

Leaf attachment petiolate. Blade attachment marginal. Laminar size microphyll; laminar shape elliptic with medial symmetrical and base symmetrical. Margin unlobed and entire. Base angle acute; base shape straight. Primary venation pinnate.

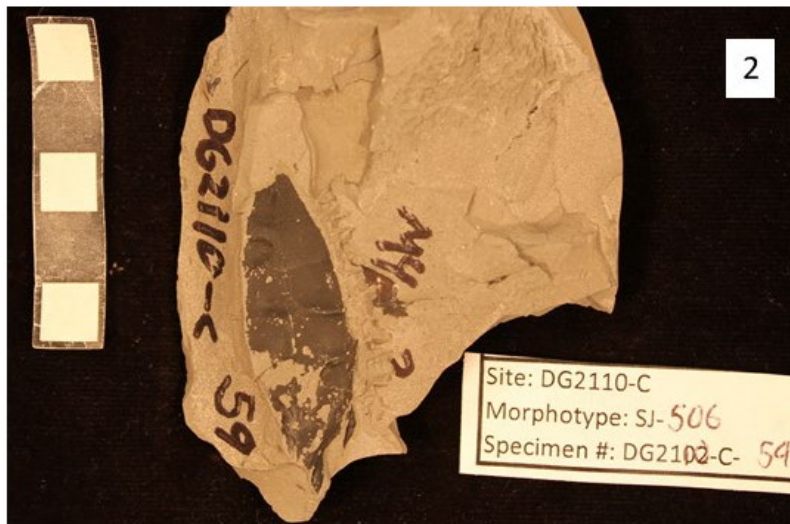


Figure A.24. Morphotype SJ-506. Present in localities DG2109 and DG2110. Specimen number: 1. DG2109-C-75, 2. DG2110-C-59.

Morphotype SJ-507 Leaf Architecture Description

Laminar size notophyll; laminar shape ovate with medial symmetrical. Margin unlobed and entire. Apex angle acute; apex shape acuminate. Primary venation pinnate; agrophic veins simple. Major secondaries simple brochidodromous, spacing decreasing proximally, smoothly decreasing proximally; attachment excurrent. Intercostal tertiary veins straight opposite percurrent to sinuous opposite percurrent.



Figure A.25. Morphotype SJ-507. Present in localities DG2102, DG2104, and DG2109. Specimen number: 1. DG2104-voucher, 2. DG2104-C-24, 3. DG2104-C-18.

Morphotype SJ-508 Leaf Architecture Description

Laminar size notophyll; laminar shape elliptic with medial symmetrical. Margin entire.

Primary venation pinnate. Major secondaries eucamptodromous, spacing irregular, uniform; attachment decurrent. Intercostal tertiary veins straight opposite percurrent to sinuous opposite percurrent; perpendicular to midvein; vein angle increasing exmedially. Epimedial tertiaries opposite percurrent; proximal course perpendicular to midvein; distal course parallel to intercostal tertiary. Exterior tertiary course looped.

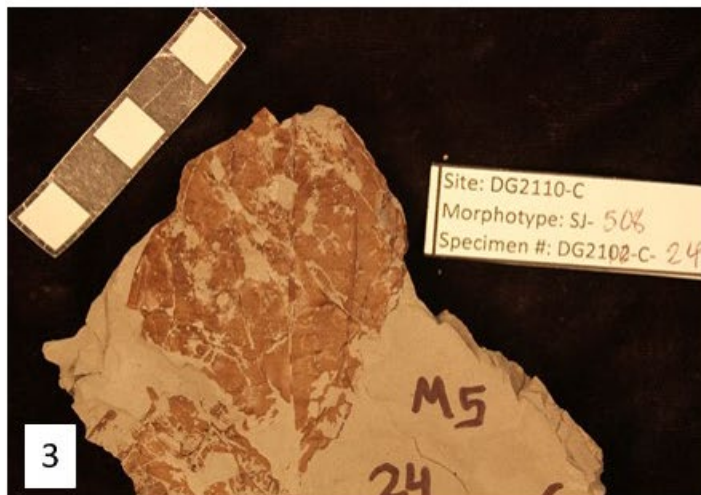


Figure A.26. Morphotype SJ-508. Present in locality DG2110. Specimen number: 1. DG2110-C-9, 2. DG2110-C-5, 3. DG2110-C-24.

Morphotype SJ-509 Leaf Architecture Description

Leaf attachment petiolate. Blade attachment marginal. Lamina shape ovate with medial symmetrical and base symmetrical. Margin unlobed and entire. Apex angle acute; base angle obtuse; base shape rounded. Primary venation pinnate. Major secondaries festooned brochidodromous, spacing irregular, smoothly increasing proximally; attachment basally decurrent. Interior secondaries present, proximal course parallel to major secondaries; occur at ~ 1 per intercostal area; Intercostal tertiary veins mixed percurrent. Quaternary vein fabric alternate percurrent. Quinternary vein fabric freely ramifying.

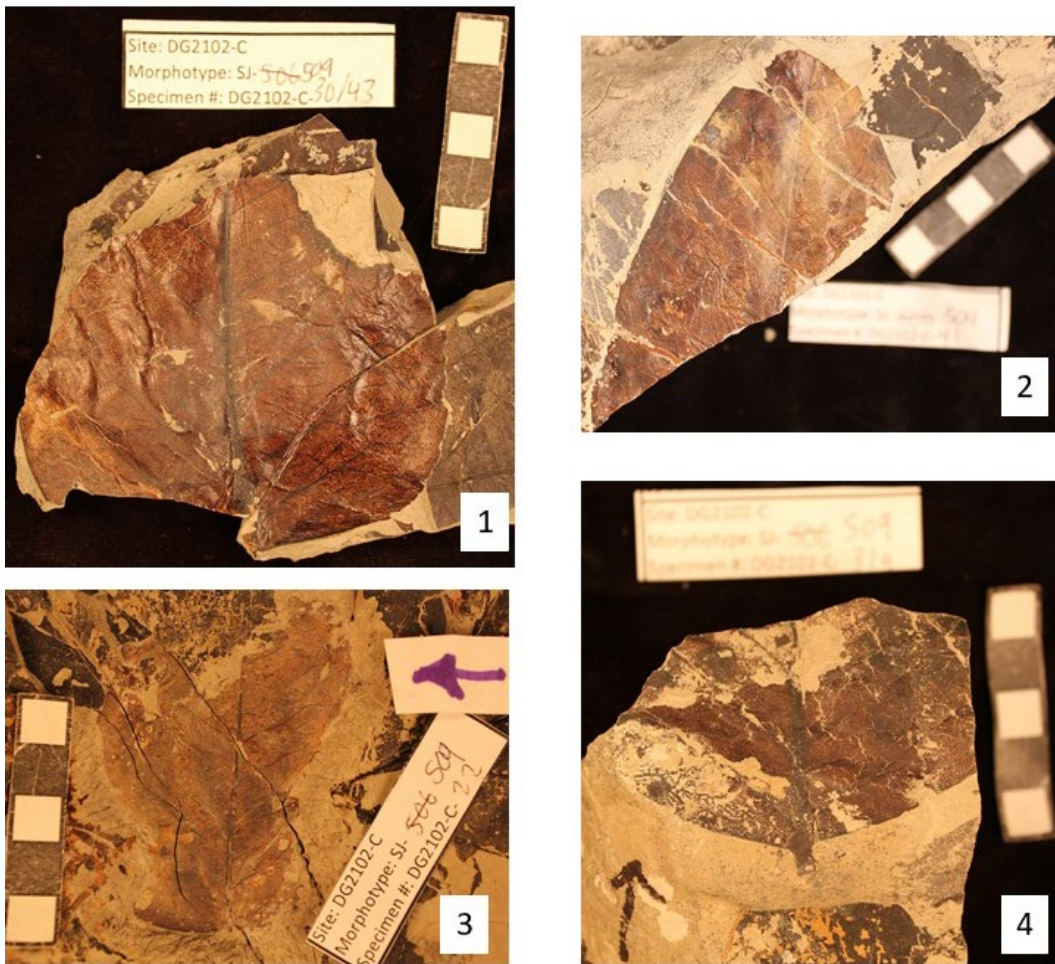


Figure A.27. Morphotype SJ-509. Present in locality DG2102. Specimen number: 1. DG2102-C-30, 2. DG2102-C-41, 3. DG2102-C-22, 4. DG2102-C-31.

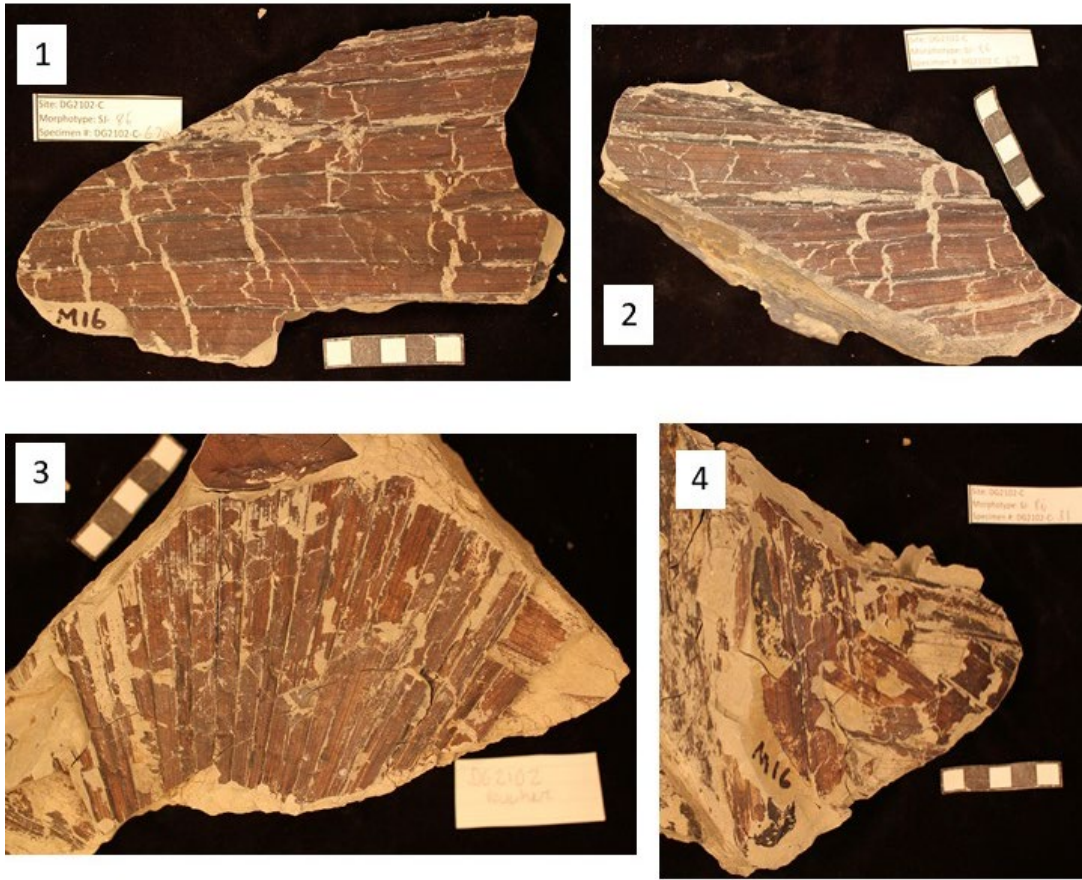


Figure A.28. Morphotype SJ-86. Present in locality DG2102. Specimen number: 1. DG2102-C-67a, 2. DG2102-C-67b, 3. DG2102-voucher, 4. DG2102-C-31. Palm frond.



Figure A.29. Morphotype SJ-57. Present in locality DG2110. Specimen number: 1. DG2110-C-20, 2. DG2110-C-23, 3. DG2110-C-42.

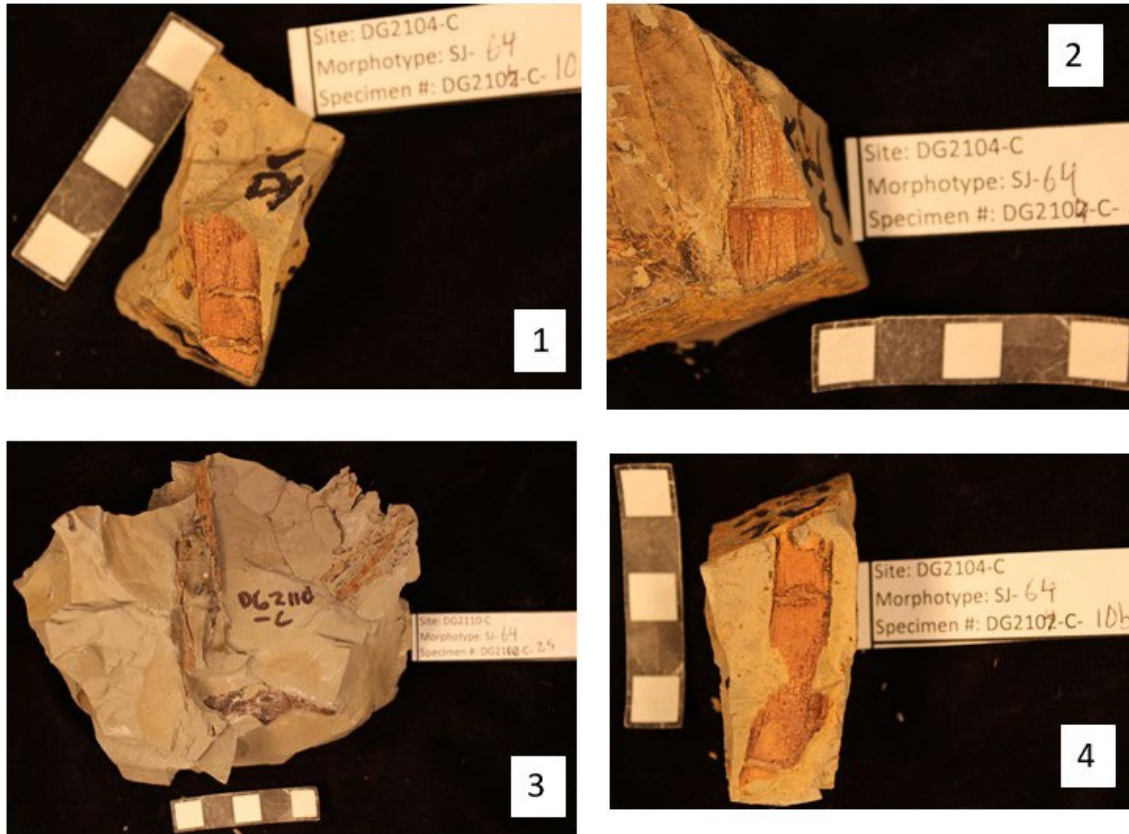


Figure A.30. Morphotype SJ-64. Present in localities DG2104 and DG2110. Specimen number: 1. DG2104-C-10, 2. DG2104-C-5, 3. DG2110-C-25, 4. DG2104-C-10b. *Equisetum*.



Figure A.31. Morphotype SJ-115. Present in locality DG2110. Specimen number: 1. DG2110-C-55a, 2. DG2110-C-9. Serrated fern.



Figure A.32. Morphotype SJ-116. Present in locality DG2104. Specimen number: 1. DG2104-C-34a, 2. DG2104-C-8a, 3. DG2104-C-13.



Figure A.33. Morphotype SJ-148. Present in locality DG2102. Specimen number: DG2102-C-58.



Figure A.34. Morphotype SJ-158. Present in locality DG2110. Specimen number: 1. DG2110-C-19, 2. DG2110-C-40, 3. DG2110-C-60.



Figure A.35. Morphotype SJ-95. Present in locality DG2109. Specimen number: 1. DG2109-voucher, 2. DG2109-C-46. *Isoetes*.



Figure A.36. Morphotype SJ-70. Present in locality DG2110. Specimen number: DG2110-C-10. Seed with small dots.



Figure A.37. Morphotype SJ-101. Present in locality DG2109. Specimen number: 1. DG2109-C-13. Assymetrical seed.

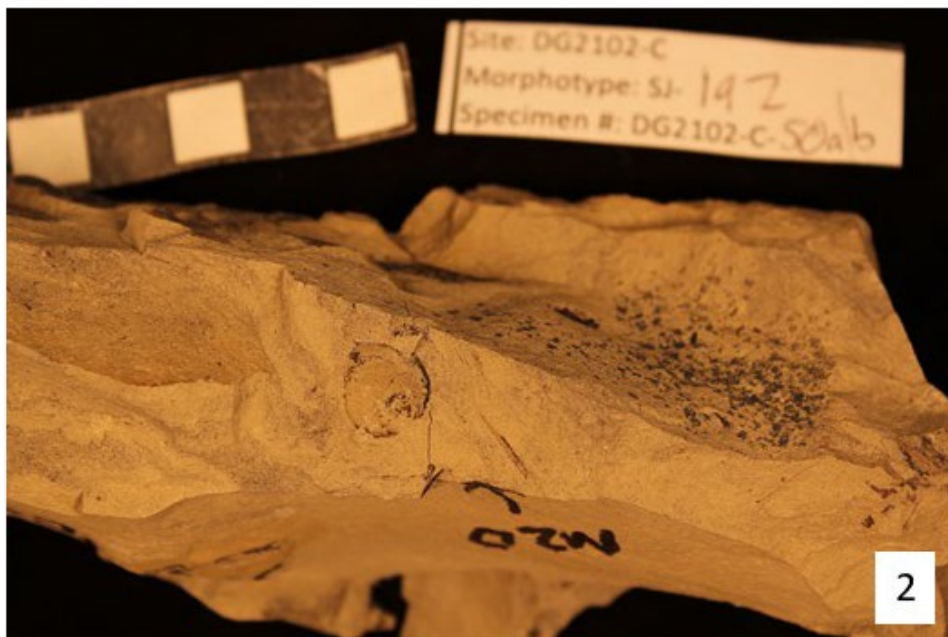


Figure A.38. Morphotype SJ-192. Present in localities DG2102 and DG2104. Specimen number: 1. DG2102-C-50, 2. DG2102-C-50.

BIBLIOGRAPHY

- Barclay, R.S., Johnson, K.R., Betterton, W.J., and Dilcher, D.L., 2003, Stratigraphy and megafloora of a K-T boundary section in the eastern Denver Basin, Colorado: *Rocky Mountain Geology*, v. 38, p. 45–71.
- Baltz, E.H., 1967, Stratigraphy and Regional Tectonic Implications of Part of Upper Cretaceous and Tertiary Rocks East-Central San Juan Basin New Mexico: *Geological Survey Professional Paper 552*.
- Baltz, E.H., Ash, S.R., and Anderson, R.Y., 1966, History of nomenclature and stratigraphy of rocks adjacent to the Cretaceous-Tertiary boundary, western San Juan Basin, New Mexico: *United States Geological Survey Professional Paper 524-D*, p. 1–23.
- Berger, W.H., and Parker, F.L., 1970, Diversity of Planktonic Foraminifera in Deep-Sea Sediments: *Science*, v. 168, p. 1345–1347.
- Brown, R.W., 1962, Paleocene Flora of the Rock Mountains and Great Plains: *United States Geological Survey Professional Paper 375*, p. 1–119.
- Buzas, M. A., and T G. Gibson, 1969, Species diversity: benthonic Foraminifera in western north Atlantic. *Science* 163:72-75.
- Cather, S.M., 2004, The Laramide orogeny in central and northern New Mexico and southern Colorado, in Mack, G.H. and Giles, K.A. eds., *The Geology of New Mexico - A Geologic History*, New Mexico Geological Society Special Publication, v. 11, p. 203–248.
- Cather, S. M., Heizler, M. T., and Williamson, T. E., 2019, Laramide fluvial evolution of the San Juan Basin, New Mexico and Colorado: Paleocurrent and detrital-sandstone age constraints from the Paleocene Nacimiento and Animas formations: *Geosphere*, v. 15, no. 15, p. 1641-1664.
- Chao, A. 1984. Nonparametric estimation of the number of classes in a population. *Scandinavian Journal of Statistics* 11:265-270.
- Chapin, C.E., and Cather, S.M., 1983, Eocene tectonics and sedimentation in the Colorado Plateau-Rocky Mountain area: *Arizona Geological Society Digest*, v.14, p. 173–198.

- Davis, A.J., Peppe, D.J., Atchley, S.C., Williamson, T.E., and Flynn, A.G., 2016, Climate and landscape reconstruction of the Arroyo Chijuilita Member of the Nacimiento Formation, San Juan Basin, New Mexico: Providing environmental context to early Paleocene mammal evolution: *Palaeogeography, Palaeoclimatology, Palaeoecology*, v. 463, p. 27–44.
- Dunn, R., 2003, Correlation of leaf megafossil and palynological data with North American land mammal ages from Paleocene-aged strata of the Ferris and Hanna Formations, Hanna Basin, south-central Wyoming: MS thesis, University of Wyoming.
- Ellis, B., et al., 2009, *Manual of leaf architecture*: Cornell University Press: Ithaca.
- Flynn, A. G., 2020, Early Paleocene fossil floras, paleoclimate and magnetostratigraphy from the San Juan Basin, New Mexico, USA. Dissertation, Baylor University.
- Flynn, A.G., Peppe, D.J., 2019, Early Paleocene tropical forest from the Ojo Alamo Sandstone, San Juan Basin, New Mexico, USA. *Paleobiology* 45(4): 612-635.
- Hammer, Ø., Harper, D.A.T., and Ryan, P.D., 2001, Past: Paleontological statistics software package for education and data analysis: *Palaeontologia Electronica*, v. 4, p. 1–9.
- Hickey, L.J., 1977. Stratigraphy and paleobotany of the Golden Valley Formation (Early Tertiary) of western North Dakota. *GSA Memoir* 150, 1–183.
- Hickey, L. J., 1980, Paleocene stratigraphy and flora of the Clark's Fork Basin: *Papers on Paleontology*, 24: 33-49.
- Huff PM, Wilf P, Azumah EJ. 2003. Digital future for paleoclimate estimation from fossil leaves? Preliminary results. *Palaios* 18: 266–274.
- Johnson, K.R., 1989, High-resolution megafloral biostratigraphy spanning the Cretaceous-Tertiary boundary in the northern Great Plains [Ph.D. Dissertation]: Yale University, 556 p.
- Johnson, K. The Hell Creek Formation and the Cretaceous-Tertiary Boundary in the Northern Great Plains: An Integrated Continental Record of the End of the Cretaceous. *Geological Society of America Special Volume* 2002.
- Johnson, K. R., Reynolds, M. L., Werth, K. W., Thomasson, J. R., 2003, Overview of the Late Cretaceous, early Paleocene, and early Eocene megafloras of the Denver Basin, Colorado: *Rocky Mountain Geology*, 38: 101-120.

- Knowlton, F.H., 1930. The flora of the Denver Basin and associate formations of Colorado. United States Geological Survey Professional Paper 155, 1–139.
- Legendre, P. & L. Legendre. 1998. Numerical Ecology, 2nd English ed. Elsevier, 853 pp.
- Leslie, C.E., et al., 2018, High-resolution magnetostratigraphy of the upper Nacimiento Formation, San Juan Basin, New Mexico, USA: Implications for basin evolution and mammalian turnover. *American Journal of Science* 318: 300-334.
- Lesquereux, L., 1878, Contributions to the Fossil Flora of the Western Territories part II, the Tertiary Flora: United States Geological Survey of the Territories, v. 7, 366 p.
- Lyson, T.R., et al., 2019. Exceptional continental record of biotic recovery after the Cretaceous–Paleogene mass extinction. *Science*, v. 366(6468), pp.977-983.
- Manchester, S.R., 1999. Biogeographical relationships of North American Tertiary floras. *Annals of the Missouri Botanical Garden* 86 (2), 472–522.
- Miller, I.M., Brandon, M.T., and Hickey, L.J., 2006, Using leaf margin analysis to estimate the mid-Cretaceous (Albian) paleolatitude of the Baja BC block: *Earth and Planetary Science Letters*, v. 245, p. 95–114.
- Newberry, J.S., 1868, Notes on the later extinct floras of North America, with descriptions of some new species of fossil plants from the Cretaceous and Tertiary strata: *Lyceum Natural History New York Annals*, v. 9, p. 1–76.
- Nichols, D.J., Ott, H.L., 1978. Biostratigraphy and evolution of the Momipites-caryapollenites lineage in the early Tertiary in the Wind River Basin, Wyoming. *Palynology* 2, 93–112.
- Peppe, D.J., 2010, Megafloral change in the early and middle Paleocene in the Williston Basin, North Dakota, USA: *Palaeogeography, Palaeoclimatology, Palaeoecology*, 298(3): 224 – 234.
- Peppe, D. J., L. J. Hickey, I. M. Miller, and W. A. Green. 2008. A morphotype catalogue, floristic analysis and stratigraphic description of the Aspen Shale flora (Cretaceous-Albian) of southwestern Wyoming. *Bulletin of the Peabody Museum of Natural History* 49:181 – 208.
- Peppe, D.J. et al., 2011a, Sensitivity of leaf size and shape to climate: global patterns and paleoclimatic applications: *New Phytologist*, v. 190, p. 724–739.
- Peppe, D.J., et al., 2018, Reconstructing paleoclimate and paleoecology using fossil leaves. In *Methods in Paleocology: Reconstructing Cenozoic Terrestrial Environments and Ecological Communities*. Springer (Vertebrate Paleobiology and Paleoanthropology Series): 289-318.

- Royer, D.L., Wilf, P., Janesko, D.A., Kowalski, E.A., and Dilcher, D.L., 2005, Correlations of climate and plant ecology to leaf size and shape: potential proxies for the fossil record: *American Journal of Botany*, v. 92, p. 1141–1151.
- Simpson, E. H., 1949. Measurement of diversity: *Nature*, v. 163, 688.
- Tidwell, W.D., Ash, S.R., and Parker, L.R., 1981, Cretaceous and Tertiary floras of the San Juan Basin, in Lucas, S.G., Rigby, J.K., and Kues, B.S. eds., *Advances in San Juan Paleontology*, Albuquerque, New Mexico, University of New Mexico Press, p. 307–332.
- Whittaker, R.H., 1975, *Communities and Ecosystems*: New York, Macmillan, 1–352 p.
- Wilf, P., 1997, When are leaves good thermometers? A new case for Leaf Margin Analysis: *Paleobiology*, v. 23, p. 373–390.
- Wilf, P., Wing, S.L., Greenwood, D.R., and Greenwood, C.L., 1998, Using fossil leaves as paleoprecipitation indicators: An Eocene example: *Geology*, v. 26, p. 203–206.
- Wilf, P. Johnson, K. 2004, Land Plant Extinction at the End of the Cretaceous: A Quatitative Analysis of the North Dakota Megafloral Record: *Paleobiology* 30(3).
- Wilf, P., et al., 2003, Correlated Terrestrial and Marine Evidence for Global Climate Changes before Mass Extinction at the Cretaceous–Paleogene Boundary. *Proceedings of Academy of Sciences*, 100.2
- Williamson, T.E., 1996, The beginning of the age of mammals in the San Juan Basin, New Mexico: Biostratigraphy and evolution of Paleocene mammals of the Nacimiento Formation: *New Mexico Museum of Natural History and Science Bulletin*, v. 8, p. 1–141.
- Williamson, T.E., and Lucas, S.G., 1992, Stratigraphy and mammalian biostratigraphy of the Paleocene Nacimiento Formation, southern San Juan Basin, New Mexico: *New Mexico Geological Society Guidebook* 43, p. 265–296.
- Williamson, T.E., et al., 2008, Paleocene palynomorph assemblages from the Nacimiento Formation, San Juan Basin, New Mexico, and their biostratigraphic significance: *New Mexico Geology*, 30: 3-11.
- Wing, S.L. and Currano, E.D., 2013. Plant response to a global greenhouse event 56 million years ago. *American Journal of Botany*, 100(7): 1234-1254.
- Wing, S.L., et al., 2005. Transient floral change and rapid global warming at the Paleocene-Eocene boundary. *Science*, 310(5750): 993-996.

Wing, S. L., Alroy, J., and Hickey, L. J., 1995, Plant and mammal diversity in the Paleocene to Early Eocene of the Bighorn Basin: Palaeogeography, Palaeoclimatology, Palaeoecology, 115: 117-155.